PRECISION MEASUREMENTS OF GAMMA-RAY WAVELENGTHS OF THE RADIUM AND THORIUM SERIES USING THE FOCUSSING CRYSTAL SPECTROMETER

Thesis by

David Joseph Klein

In Partial Fulfillment of the Requirements

for the Degree of

Doctor of Philosophy

California Institute of Technology

Pasadena, California

1951

Table of Contents

Table of Contents

Illustrations

Illustrations

Tables

Plates

Acknowledgments

The helpful advice and encouragement of Prof. Jesse W.M. DuMond as supervisor of this work is gratefully acknowledged.

David E. Muller, James R. Brown and Dr. David A. Lind rendered able assistance in the adjustment and operation of the spectrometer, and in discussions of the work.

We are indebted to Dr. Clyde K. Emery of the Emery Tumor Group, Los Angeles, for supplying the rather large amount of radon gas which was used, and to Dr. Gordon L. Locher for versatile handling of the radon pumping plant and for advice in the preparation of the sources.

Prof. N. F. Ramsey and Prof. R. B. Holt of the Nuclear Laboratory, Harvard University, expedited the loan of the 150 mc source of radiothorium.

Certain illustrations were taken from the theses of Mr. Muller and Mr. Brown, and from the Quarterly Reports of Prof. DuMond.

This investigation was supported in part by the Office of Naval Research and the Atomic Energy Commission, under Contract No. N6onr-244, Task Order IV.

Abstract

The curved crystal spectrometer is described very briefly. The preparation and mounting of sources of radon and radiothorium for use in the instrument is described. Certain calculations of line profiles to be observed are carried out and a graphical method is given which permits rapid estimate of the important features of the profile as functions of the source geometry. The construction of multicellular Geiger counters and measurements of their efficiency are described. The results of precision measurements of five gamma-ray lines and one x-ray line of the radium spectrum are given, as well as those of six gamma-ray lines of the thorium spectrum.

I

PREVIOUS WORK ON THE GAMMA-RAY SPECTROSCOPY OF THE NATURAL RADIOELEMENTS USING CRYSTAL DIFFRACTION

The energies of nuclear gamma rays have been studied through the use of the following properties of gamma radiation:

(1) Absorption of the rays in passing through matter.

(2) Photoelectric methods.

  (a) Natural beta-spectra, excited by internal conversion of the gamma rays, i.e., the ejection of a beta ray in lieu of a gamma ray.

  (b) External conversion, the photoelectric emission of an electron from an atom other than the one emitting the gamma ray.

(3) The Compton effect.

(4) Diffraction of the gamma ray by a crystal lattice. The present work, measurement by crystal diffraction, has been preceded by other work using crystal diffraction, which will be mentioned briefly.

The earliest work was that of Rutherford and Andrade[1] in which the same apparatus was used in two ways (fig. 1). At a certain distance a from the axis of the apparatus, gamma rays of a certain wavelength from source S undergo partial diffraction in the crystal DD' some of them being bent into the beam AB, and others continuing in the direction AC. A photographic plate (EE') shows darkening throughout its area due to absorption of gamma rays of perhaps several wavelengths issuing in all directions from the source. Superposed

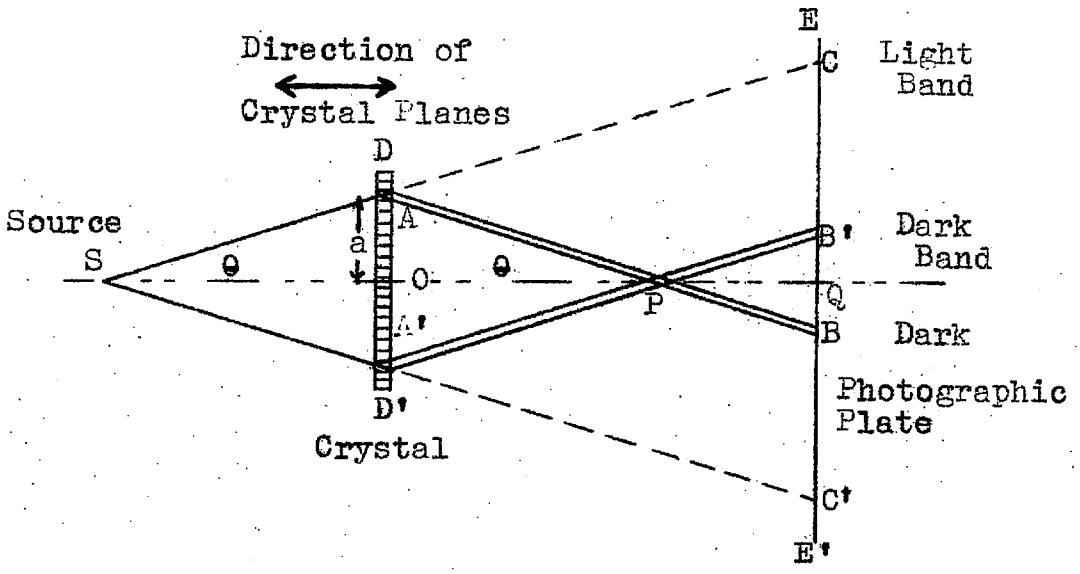

Fig. 1. Apparatus of Rutherford and Andrade.

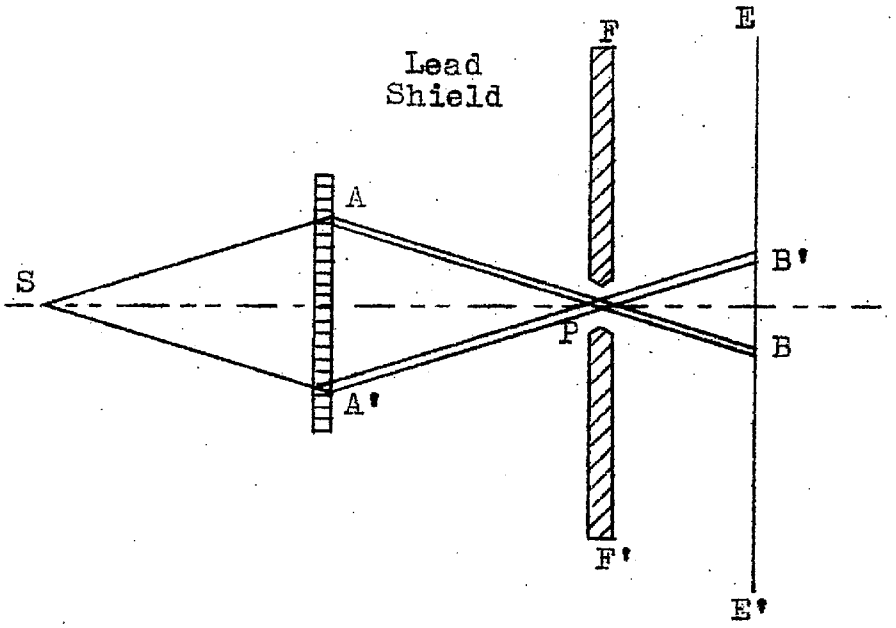

Fig. 2. Modification of apparatus of Rutherford and Andrade. Through the use of a shield with a slit, the extinction lines are sacrificed for a large reduction in background darkening of the plate.

upon this general background, there could appear a pair of light bands, C and C', caused by the diminution of the beams SAC and SA'C' because of the selective diffraction of some of the gamma rays of the given wavelength (extinction lines) and there could appear dark bands at B and B' from the diffracted gamma rays. Using the Bragg law

$$n\lambda = 2d \sin \theta_i; \quad \theta_i = \theta_d \qquad \text{eq. (1)}$$

where λ is the wavelength, d the crystal spacing, θ_i the angle between the crystal planes of interest and the incident beam, θ_d the angle between the crystal planes and the diffracted beam, and n an integer expressing the order of diffraction, together with the simple geometrical properties of the experiment; it is possible to calculate from the location of these bands the wavelength of the radiation which they represent. The light bands, being separated by a greater distance, are capable of producing the more precise measurements.

However, if the background is high due to radiation of several energies, the light bands do not survive. A simple modification (fig. 2) of this experiment is capable of bringing out more contrast in the dark lines. In this case the lead slit FF' has been added at P. By this means, the background has been eliminated except in the center of the photographic plate, at Q. Only the dark bands B and B' appear, and they no longer compete with background. This form of the experiment is more appropiate for detection of the weaker lines.

Another crystal diffraction method, used by Frilley[2] and Valadares[3] makes use of a rotating crystal (fig. 3). The crystal is mounted in such a way as to rotate about a vertical axis lying

in its face. When the Bragg laws (eq. 1) are satisfied, part of the beam emerging from the collimator is diffracted through the angle 2θ and registers as a dark band on the photographic plate. The crystal is turned slowly, of the order of one degree in four hours, and with exposures of the order of one to ten days the spectrum can be recorded on the plate. This method is capable of higher resolution and detection of higher energy radiation, but it requires very careful alignment of the apparatus and careful study of errors, particularly in order to establish the zero wavelength position on the photographic plate.

Using these methods, Valadares was able to make measurements of most of the stronger x-ray lines of the radium and thorium families, and Frilley was able to extend the measurements to the nuclear lines, even to the point of detecting the 2.18 MeV line of RaC. Precisions were limited by uncertainties in the measurements of the plates; Valadares estimates his precision to be of the order one part in 600 for the strong x-ray lines in which they were able to detect higher order reflections, while Frilley gives 0.5% precision for the longer wave lines (x-ray lines), and 2-3% precision for the short wavelength gamma rays.

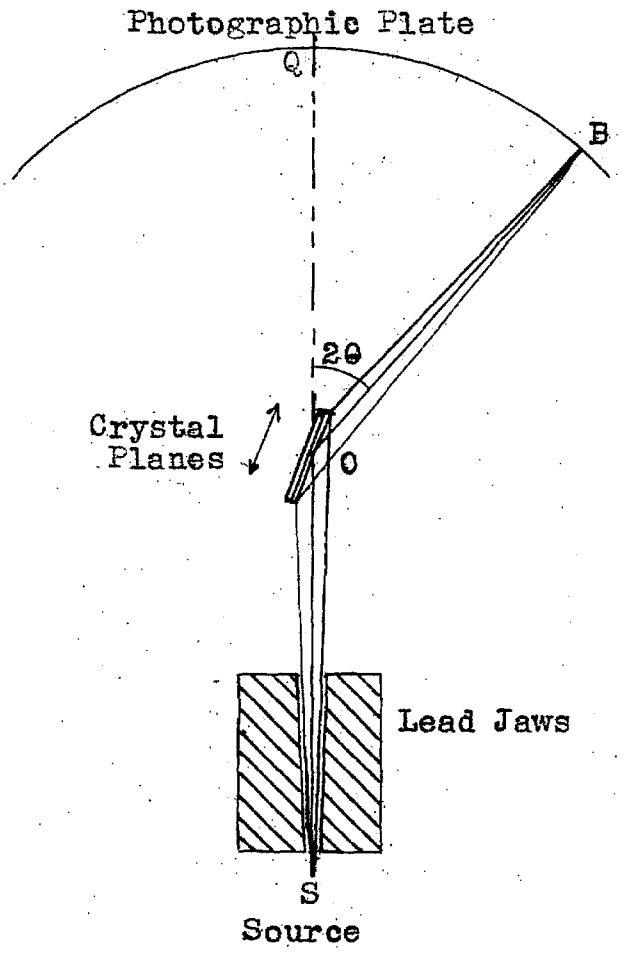

Fig. 3. Rotating crystal spectrometer as used by Frilley. A lead collimator shields the photographic plate from undiffracted radiation. If SO=OQ and the plate lies on a circular cylinder about O, the rays will be focused at B as the crystal turns (Bragg focussing). O, the axis of the crystal, lies in its face.

II

GENERAL DESCRIPTION OF THE CURVED CRYSTAL FOCUSSING SPECTROMETER

The curved crystal spectrometer has been described elsewhere[4,5], and will not be explained in detail here. As an aid to understanding the remainder of this work, a schematic diagram of the spectrometer is presented in fig.4. Briefly the operation of the spectrometer is as follows: The source of gamma rays under investigation is placed at S (fig. 4), surrounded by a lead shield and lead jaws to protect personnel and reduce background radiation. The radiation of interest passes out of an opening in the shield to the crystal at P. If the two Bragg conditions are satisfied,

$$n\lambda = 2d \sin \theta_i; \quad \theta_i = \theta_d \qquad \text{eq. (1)}$$

where n is an integer, λ the wavelength of the radiation, d the inter-atomic-plane distance, θ_i the angle between the incident direction and the crystal planes, and θ_d the angle between the diffracted direction and these planes, a small amount of the radiation will undergo diffraction. (The planes utilized are the (510) planes of quartz $d_{18^\circ} = 1177.64$ XU Siegbahn). The spectrometer satisfies the second condition automatically by virtue of its design; the planes are normal to the crystal face and the kinematics is such that by turning the crystal through half the angle through which the source is turned (about the point P), the angle between the crystal planes and the source is kept equal to the angle between the planes and the axis of the collimator. Thus the collimator is always in a position to receive the diffracted radiation from the (510) planes. The purpose of the collimator is to shield the detector from stray

SCHEMATIC DIAGRAM OF SPECTROMETER

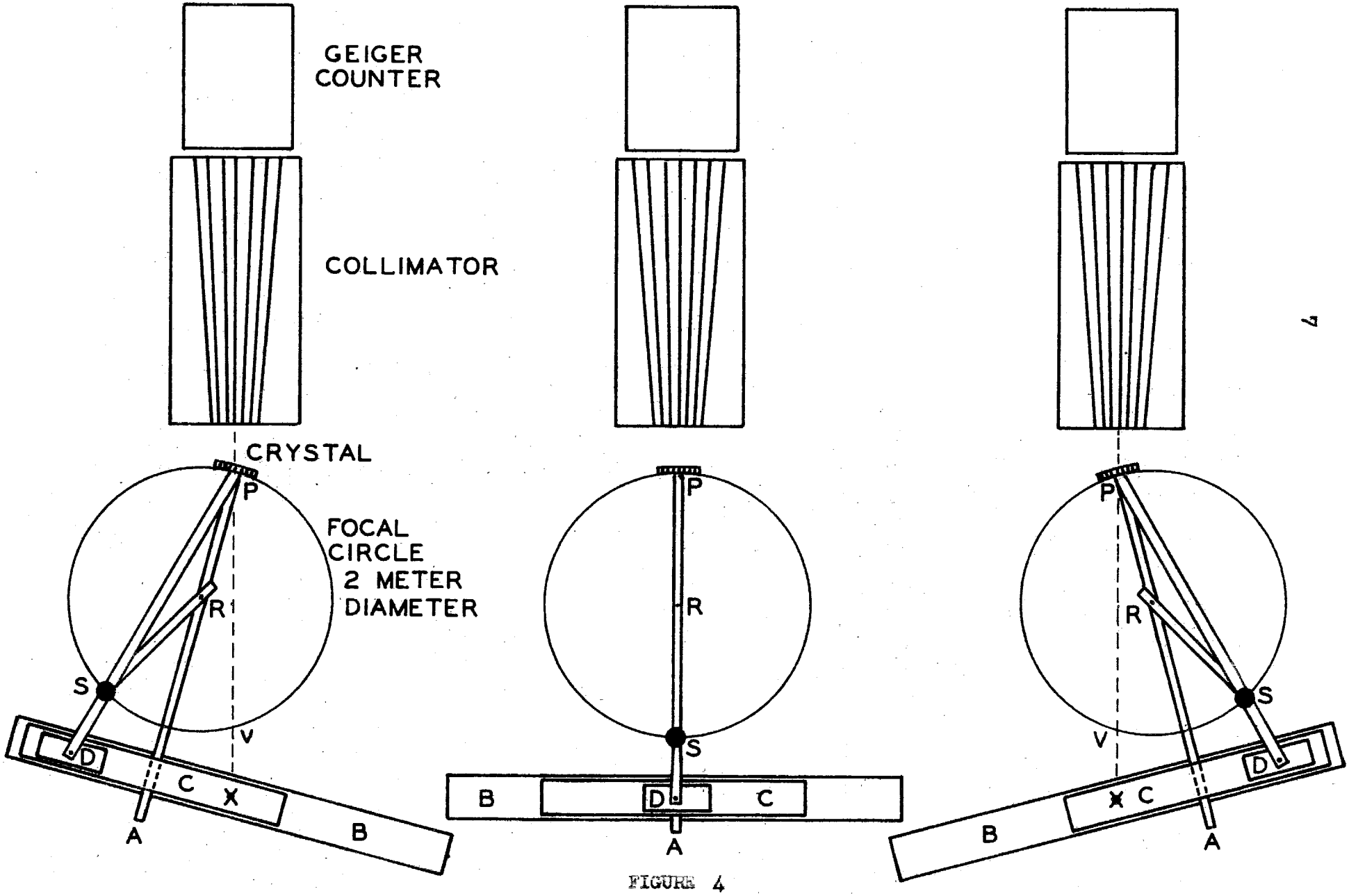

FIGURE 4

radiation and particularly from the main beam transmitted directly through the crystal when working at small angles. It is designed to offer the maximum protection possible from radiation in directions other than its axial direction, while presenting as much opening as possible to diffracted radiation. It does <u>not</u> influence the resolution of the instrument, for its "window", the range of angular directions which it will pass, is far larger, by a factor of the order 200, than the angle subtended by the source at the crystal. This subtended angle, usually of the order 10^{-4} radians, together with the size of the diffraction and aberration pattern of the crystal limit the resolution. If a source of the order of a centimeter in width were installed, the collimator would then determine the resolution, and the instrument would be indeed poor by comparison with other nuclear spectrometers.

The resolution is constant in wavelength for a given source, and is of the order 0.1 milliangstroms. The precision is of the order 0.01 milliangstroms. At 0.5 MeV, which can be considered a median working energy for the instrument, this represents a resolution of about 1 part in 250, and precision of about 1 part in 2500. At this energy the angle θ mentioned above is about 0.7 degrees, so that it is difficult to see the angular displacement of the beam from the central position. This points up the necessity of a good collimator, for the main beam and diffracted beam are less than a degree apart and, due to the low reflecting power of the crystal (proportional to λ^2) the main beam is thousands of times stronger than the diffracted beam.

The kinematic motion of the machine was very carefully designed by Prof. J. W. M. DuMond and described in a paper by him[4]. These parts are indicated as the carriages B, C, D, the beams AP and SP, and the linkage SR. The geometry will not be described here but it results in a motion for which wavelength setting in milliangstroms is very closely equal to turns of a screw. The dial is graduated so that with a vernier it can be read to the nearest thousandth of a turn (thousandth of a milliangstrom).

A unique feature of the transmission type spectrometer is the fact that a line can be detected and measured on both sides of center. This eliminates the difficulty of ascertaining accurately the center of the instrument scale, a problem which created trouble for Frilley and others. This central position can change slightly every time a source is installed, for the source may be inaccurately placed. By subtracting readings on the two sides, a value of twice the wavelength is obtained with no loss of accuracy, for the doubling of the time of run occasioned by making runs on both sides can be shown to result in an improvement of $\sqrt{2}$ in accuracy (due to counting) just as would be gained if twice as long a run were made on one side and the center were accurately known.

The curved crystal spectrometer has a luminosity small compared with that of other instruments. Sources of 50 millicuries or larger are usually required but some fairly good runs have been made with only 10 mc of Rn. The problem of intensity will not be further discussed here but components of it are discussed in other chapters.

III

DESIGN OF THE SOURCE HOLDER AND PREPARATION OF SOURCE SAMPLES

The preparation of the source samples and their mounting in the spectrometer presented two quite different problems in the case of radon and in the case of radiothorium. This results from the fact that radon exists as a gas with a short half-life (3.8 days), which can be compressed into a small volume if it is sufficiently pure, while radiothorium, with a long half-life (1.9 years) cannot possess as high a specific activity, is very expensive, and its fabrication into a special shape is a difficult and dangerous task.

3.1 Preparation of Radon Sources

Radon sources were prepared in a fashion quite similar to that of producing radon seeds for medical therapy. Aluminum tubing was drawn to a specific size and filled with the gas in a radon pumping plant.

Purification of the gas was accomplished by the usual methods, using established together with new techniques for burning all the hydrogen, absorbing carbon dioxide and other gases in a zirconium purifier, absorbing moisture in phosphorous pentoxide or potassium hydroxide, freezing the radon in a liquid nitrogen trap and pumping away the gases, and finally fractionating off the lighter gases using liquid nitrogen to cool the aluminum tube. It is to be remarked that even with these extensive purification procedures, the mixture admitted to the aluminum tube consists largely of impurities, with only a small fraction of radon, by volume.

Two types of tubes were prepared and used, whose cross sections are shown in figure 5. In the first case, the round tubing was drawn to 0.80 mm outside diameter by hand, starting with 1/8" soft aluminum tubing. In the second case, the 1/8" tubing was drawn to 1.5 mm o.d. A section of each piece was then further drawn to 0.80 mm in order to form a nipple which could be attached to the pumping plant. The large section was then squeezed to the oval cross section shown, between parallel blocks of steel. After the tube filled with radon was separated from the vacuum system, the radon could be concentrated into the desired section of the tube, using liquid nitrogen, and this section could be cut off to a length of about 35 millimeters, the proper length of source for use in the spectrometer.

Aluminum was chosen for its low absorption of gamma rays, consistent with good mechanical properties at room temperature and at liquid gas temperatures. The pumping system had been intended to fill gold tubing, but in the most critical case, that of the 52.8 KeV line, the gold tubing transmits approximately 3% of this soft radiation, while aluminum tubing of the same dimensions transmits 97%. On the other hand, aluminum and gold share the property of work-hardening, which was essential in making a tight seal on the end of the tube in the operation of nipping it off.

As was mentioned in Chapter II, the resolution of the spectrometer is limited principally by crystal aberrations and by the width of the source or source slit, whichever may be smaller. Since, however, the aberrations result in a line width of 0.16 XU at half maximum, as determined by measurement[6] of the 411 KeV line of Au^{198} (fig. 9)

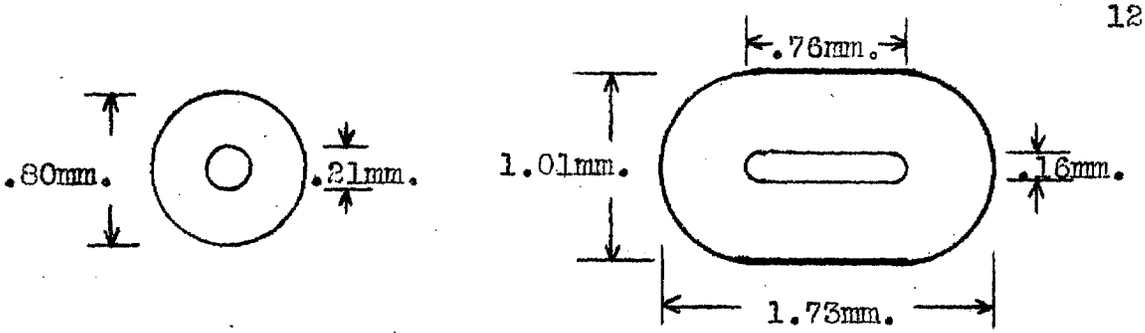

Fig. 5. Cross-section of tubes in which the radon was collected. The flat tube (right) afforded more volume for the incidental gaseous impurities, at the same time presenting a narrower (0.16mm.) source to the instrument. The tubes were cut approximately 1¼" long.

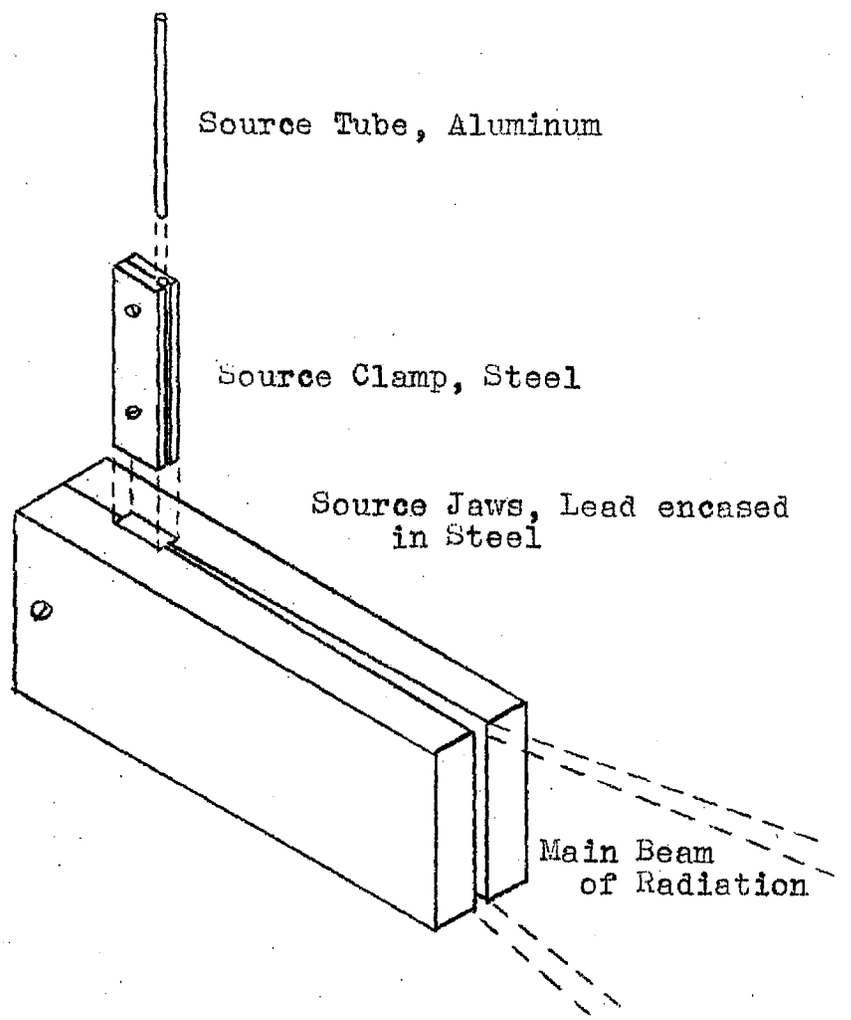

Fig. 6. Exploded view of mounting of radon in the spectrometer. The use of a separate source clamp insures automatic alignment of the active source.

whose natural spectral breadth is completely negligible, and since 1 mm width at the source represents approximately 1 milliangstrom spread in wavelength, it is profitable from the standpoint of resolution to reduce the width to 0.2 mm, but any further reduction in width will have little value, for the crystal aberrations will spread the rays anyway. Since we are limited in the total amount of radon yield available in one pumping which sets a limit to the size of the integrated line profile as compared with background, if the source can be compressed into a width of 0.1 mm, the resulting line profile will be high and narrow, giving good counting statistics in the presence of background, and the resulting portions of high slope will be an aid in the precise determination of its position.

Using the round tubing with inside diameter about 0.15 mm, it became difficult to compress 150 millicuries of Rn and its associated impurities into the required small volume. It was for this reason that the change was made to flattened tubing. The flattened tubing contained approximately five times as much volume as the round tubing.

After the tube was filled with radon and trimmed to the desired length, it was clamped in a source clamp machined for this purpose. This assembly could then be slipped into the chamber of the source jaws, which had previously been mounted on the spectrometer source table, ascertained to be perpendicular to the source table, and visually aligned with the center of the crystal (fig. 6).

3.2 Mounting of the Radiothorium Source

Calculations of intensity have indicated that ${}_{88}MsTh_1^{228}$ (6.7 year isotope of Ra) and ${}_{90}RdTh^{228}$ (1.9 year isotope of Th) are possible sources to be investigated in the curved-crystal spectrometer. In

the thorium disintegration series, gamma rays accompany the following disintegrations[7]:

$$_{87}MsTh_2^{228} \longrightarrow {}_{88}RdTh^{228} + \beta \quad (1)$$

$$_{88}RdTh^{228} \longrightarrow {}_{86}ThX^{224} + \alpha \quad (2)$$

$$_{82}ThB^{212} \longrightarrow {}_{83}ThC^{212} + \beta \quad (3)$$

$$_{83}ThC^{212} \longrightarrow {}_{84}ThC'^{212} + \beta \quad (4)$$

$$_{83}ThC^{212} \longrightarrow {}_{81}ThC''^{208} + \alpha \quad (5)$$

$$_{81}ThC''^{208} \longrightarrow {}_{82}ThD^{208} + \beta \quad (6)$$

A source of MsTh in equilibrium with its products would have the possibility of emitting the gamma rays of all six of the above transitions, while a source of RdTh would not give the gamma rays accompanying transition (1). On the other hand if a source of $MsTh_1$ were to be fabricated to order, it is likely that it would not be in secular equilibrium, so that a separate source of RdTh would be required in order to study gamma rays subsequent to reaction (2). Since β-ray spectroscopy makes use of the active deposit of the thorium emanation $_{86}Tn^{220}$ for purposes of calibration, the gamma rays subsequent to (3) have practical significance.

In the light of these considerations, the high cost of fabrication of these kinds of sources ruled out the use of MsTh for the present, at least until the supply of less expensive but important neutron-activated sources has been investigated, and also made it expedient to search for a ready source of RdTh which could be used on a loan basis. This search was rewarded in the form of the RdTh source[8,9] of approximately 150 mc. which is owned by ONR Contract N5 ORI-78 Task Order No. IV NR - 026-012 of the Radiation Laboratory, Harvard

University, and very kindly loaned to this task by Dr. R. B. Holt and Dr. N. F. Ramsey of that laboratory.

This source of RdTh (fig. 7) suffers from three disadvantages: (a) Its shape is not suited to the special needs of the spectrometer, (b) it is sealed in a capsule of platinum-iridium of such thickness as to cause serious attenuation of the low and medium energy gamma rays, and (c) the carrier is ThO_2, ordinary thorium, which is very highly absorbing to the low energy lines by virtue of its high atomic number. Since the operation of transferring the radioactive material to a better suited container would be a hazardous one, it was thought more feasible to "stop down" this sample with a slit and attempt to obtain as much information as possible in this manner. This procedure suffers from the fact that the effective strength of the source is reduced by a substantial factor, perhaps 5, while the background radiation due to presence of the source in the laboratory is not reduced to the same degree by the slit jaws. The latter effect is particularly strong in RdTh because of the difficulty of shielding the 2.62 MeV strong line.

A further difficulty occurs in the use of slit jaws for high energy radiation, in that it is virtually impossible to find a material of high enough absorption to make a sharp definition of the beam. The problem becomes of such importance that a careful design of the slit is justified. This analysis was undertaken by Harry C. Hoyt and David E. Muller of this laboratory in connection with the remeasurement of annihilation radiation, and will not be explained in detail here. The conclusion was reached, however, that a slit with sharp

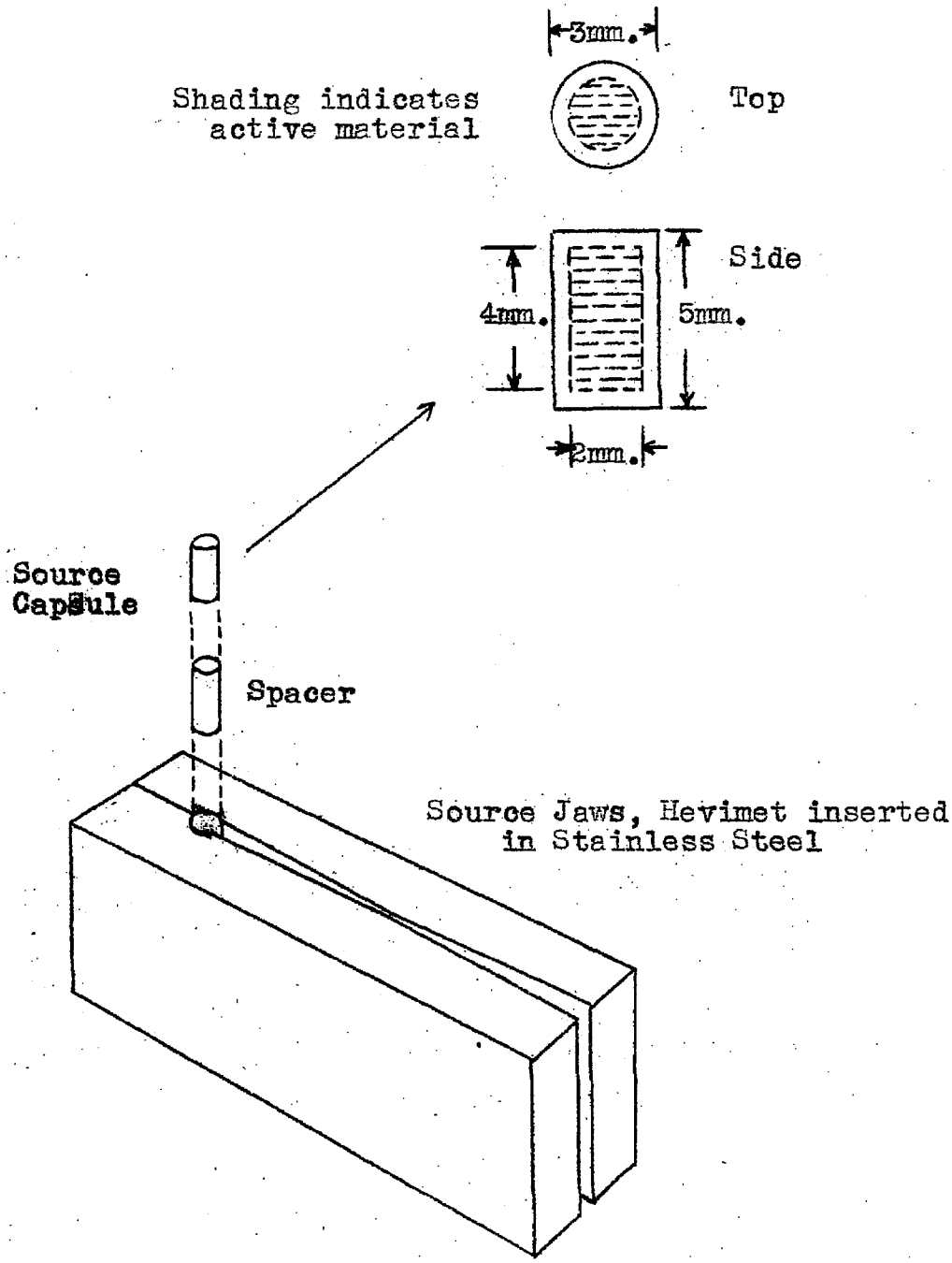

Fig. 7. Radiothorium source capsule and mount. The spacer is necessary to hold the capsule centered at the level of the center of the crystal

edges (fig. 8) cannot be surpassed for defining a divergent beam of high energy radiation. It is evident that the material of which the slit is made should have the highest linear absorption possible for the radiation of interest. If the source is very wide, the best use is made of the absorbing material if the slit gap is placed midway (in a fore-and-aft direction) between the source and the forward opening of the source holder.

The material of which the slit is fabricated is the sintered mixture developed by General Electric Company under the trade name Hevimet, of the following composition (by weight):

90% Tungsten

6% Nickel

4% Copper

The mixture of powdered metals is compressed in a mold by means of a hydraulic press, to a pressure of 80,000 p.s.i., then sintered in a refractory furnace at a temperature slightly above the melting point of copper and allowed to cool. This task is heavily indebted to Professor Pol Duwez of this Institute for very kindly preparing and sintering three blocks of the alloy. The physical properties are roughly the following: Density 18.58 g/cm^3, color gray, and machining properties resembling those of cast semi-steel, including grinding.

The jaws containing the slit are shown in perspective in figure 7, and in more detail in figure 8. They consist of stainless steel blocks with "Hevimet" inserts, and they were ground by machine, with great care taken to make the outside surfaces accurately parallel and perpendicular, as the case may be. This facilitates lining up

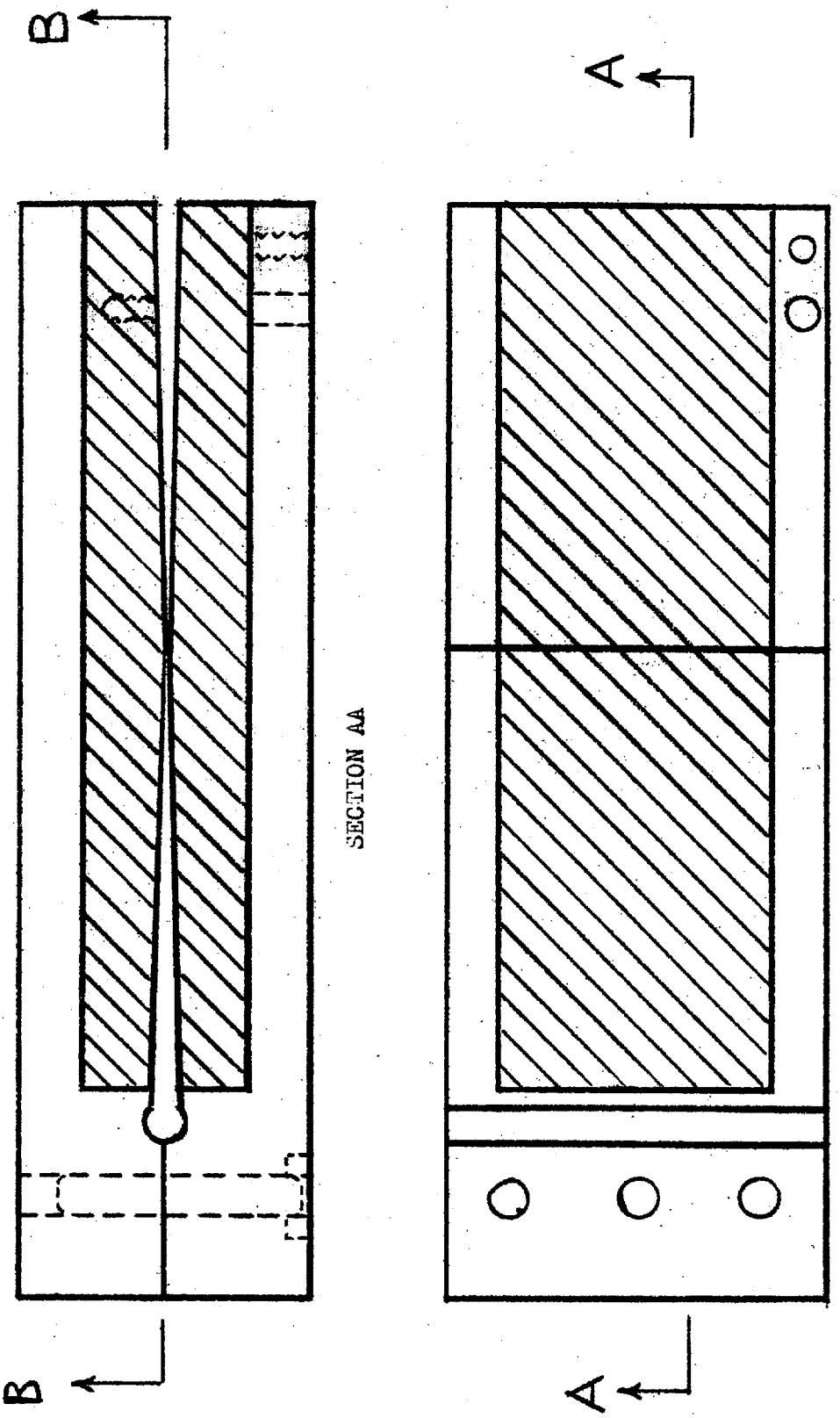

Fig. 8. Slit jaws for the radiothorium source

the slit on the spectrometer source table, in order to make it accurately parallel to the generators of the cylinder into which the crystal is bent. Adjustment screws are provided to vary the width of the slit, which can be closed completely or opened to any reasonable width using shims or spacers behind the source.

After the size of the slit is adjusted using a feeler gage, the jaws are mounted on the spectrometer source table and aligned as in the case of the radon. The capsule of radiothorium is then slipped into the chamber in such a way as to rest on a spacer, at the correct height above the source table.

Plate 1

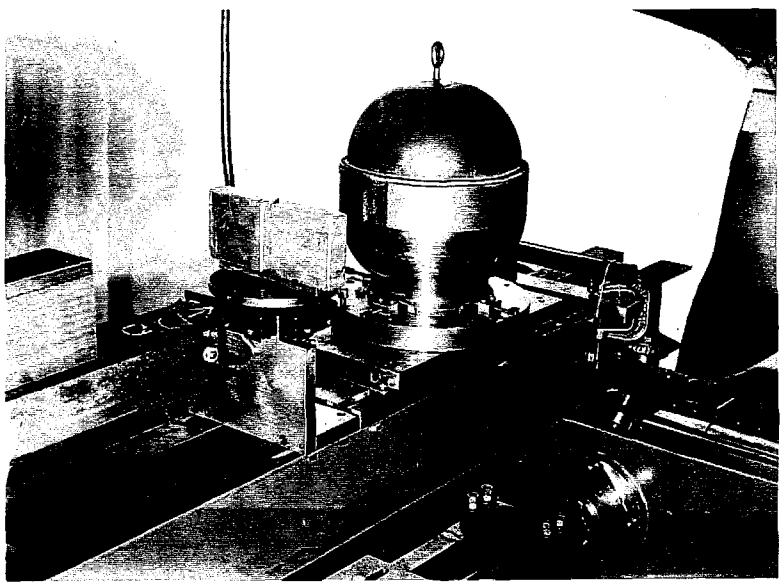

Source Bomb and Robot Operated Shutter for Background Measurement. The source bomb with lifting hook in its hemispherical lead cover can be seen on its ball-bearing rotary and translatory carriages supported on the upper beam of the spectrometer. To its left is the robot operated shutter consisting of two lead blocks between which the beam normally passes. The beam is cut off when a motor rotates this through 90°. The precision screw carriage and part of the lower beam can be seen in the lower right hand corner of this view.

IV

THE LINE PROFILE

4.1 Introduction

It has been pointed out by DuMond and Lind[5] that the shape of the line which is observed in the curved crystal spectrometer can be represented as the fold, in a sense which will be described, of the following functions of the angle of spectrometer beam:

(1) The function representing the response of the crystal to essentially monochromatic radiation emitted from an infinitesimally thin line located at a representative focus of the crystal. This curve which we frequently call the "window" curve of the crystal has features contributed by the reflection laws ("dynamical" theory of selective reflection), plus features contributed by the aberrations of focus of the crystal, and was best measured[6] by the use of a very thin source of Au^{198}. Its dependence on the precision to which an individual crystal is ground and mounted so as to be bent to a circular cylindrical shape makes this curve difficult to calculate theoretically. The observed curve is here reproduced (fig. 9). For calculation purposes it will be represented by a Gaussian function of half-width at half-maximum .08 mm travel of the carriage (.08 milliangstroms on the scale).

(2) The function representing the shape of the source, as seen by the crystal. Features of this function are

contributed by the following:

(a) The width and shape in horizontal cross-section of the source,

(b) If a slit is used to define a broad source, the shape of the slit and the effect of penetration of its edges by the radiation of interest,

(c) Possibility that the source may be inaccurately placed.

These effects, as they apply to the present case, will be discussed below.

(3) Any inhomogeneity in the wavelength of the radiation of interest, such as natural line width, structure of the line, Doppler shift or degrading of radiation in Compton scattering. Three cases have thus far been encountered in the operation of the gamma-ray crystal spectrometer:

(a) Nuclear gamma-ray lines represent the most common case. Their width is completely negligible as compared with the instrumental width.

(b) X-ray lines have an appreciable width.

(c) The annihilation radiation has an appreciable width, and has been discussed at some length[5].

We shall now calculate certain line profiles, and attempt to compare them with the experimental results.

4.2 Definition and Method of Folding of the Window Functions

Let us consider a source of some definite shape, so that not all points of its surface, as presented to the crystal, radiate

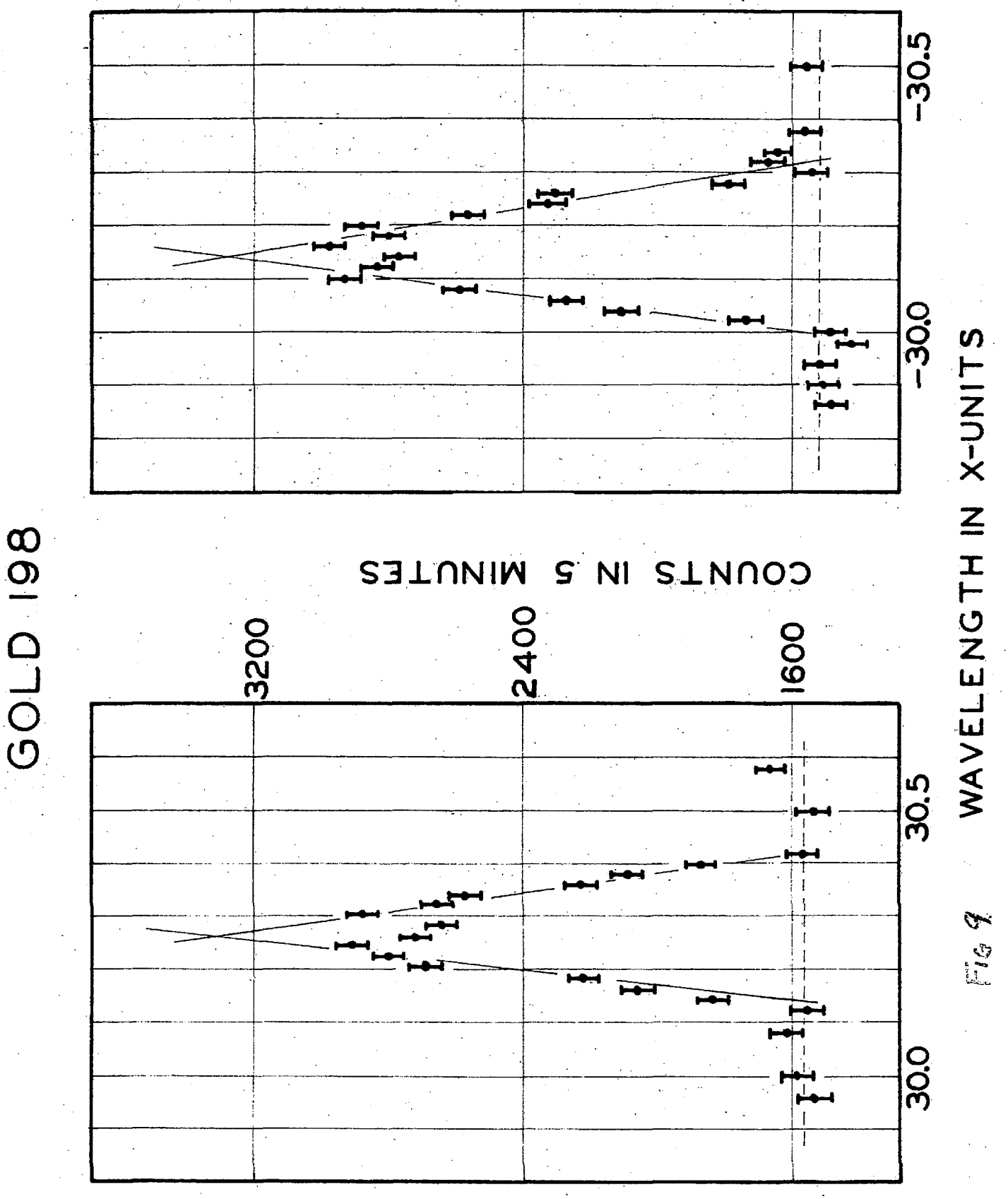
GOLD 198
COUNTS IN 5 MINUTES
3200
2400
1600
30.5
30.0
-30.5
-30.0
WAVELENGTH IN X-UNITS

Fig 9

at the same intensity. We can characterize each point of the source by the angle ξ which it makes at the crystal with respect to some reference line OA, preferably the axis of the source (fig. 10). Now let us define a function $\phi_s(\xi)$ which is proportional to the total intensity of radiation of a certain energy of interest, emitted by points characterized by ξ, and arriving at the crystal. The total radiation striking the crystal will evidently be proportional to $\int \phi_s(\xi) d\xi$, integrated over the whole source.

We can also define a function $\phi_c(\eta)$ as the relative reflectivity (for selective reflection) of the crystal to rays of our given energy approaching the crystal at an angle η (fig. 10) from the crystal focus. This crystal focus is on the focal circle on a line at an angle θ to the normal of the crystal, as shown in the figure.

These functions can be redefined as follows: If we let $z = \xi r$ and $y = \eta r$, where r is the distance from the crystal to the center of carriage C (fig. 4) for the wavelength setting of interest, and if we let $\phi_s(\xi) = f_s(z)$ and $\phi_c(\eta) = f_c(y)$ (r is sensibly constant throughout the discussion since ξ, η are always very small) then we call $f_s(z)$ the source window and $f_c(y)$ the crystal window. z and y can now be measured in turns of the spectrometer screw (milliangstroms). f_c and f_s can be normalized at will.

If the setting of the spectrometer is such that the distance between the crystal focus and the axis of the source is x measured at the screw carriage (fig. 10), the amount of reflected radiation will be proportional to

$$f_p(x) = \int_{-\infty}^{\infty} f_s(z)\, f_c(z-x)\, dz, \qquad (1)$$

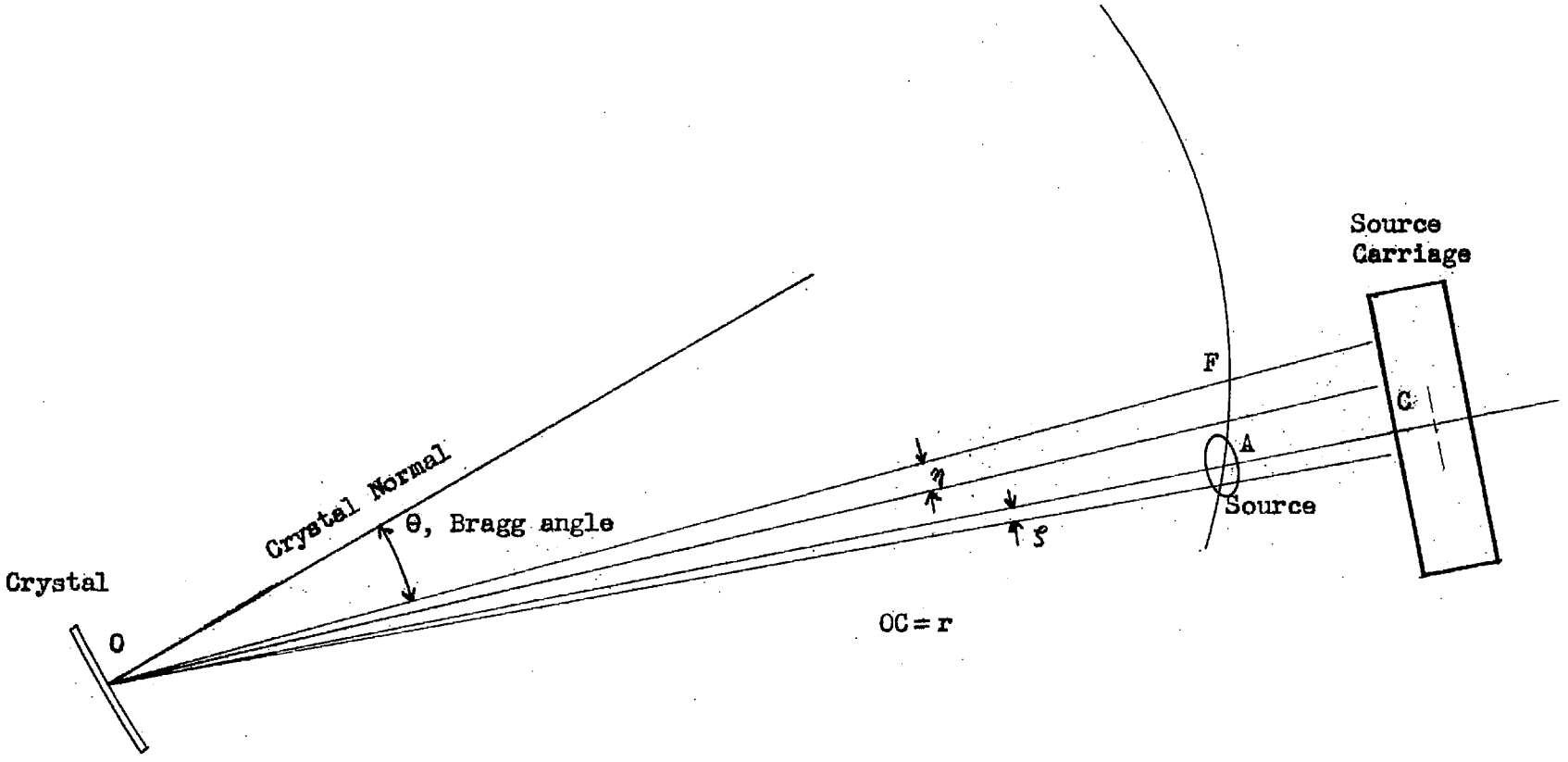

Fig. 10 The geometry of the source and crystal window functions.

Naturally both f_s and f_c have values which are substantially non-zero only for rather small values of their arguments. f_p is the line profile, and the integral shows the type of fold from which it results.

If we use the following notation for the Fourier transform of f(x):

$$\overline{f}\,(s) = \frac{1}{\sqrt{2\pi}} \int_{-\infty}^{\infty} e^{isx} f(x)\,dx, \qquad (2)$$

then the inverse transform is, for all of our cases, where $f(x) \longrightarrow 0$ rapidly as $x \longrightarrow \infty$,

$$f(x) = \frac{1}{\sqrt{2\pi}} \int_{-\infty}^{\infty} e^{-isx}\, \overline{f}\,(s)\,ds. \qquad (3)$$

In terms of this notation, the Fourier transform of the line profile is given by

$$\overline{f_p}\,(s) = \overline{f_s}\,(s)\ \overline{f_c}\,(s) \qquad (4)$$

and the method of calculating the line profile from the component windows consists in finding the transforms of the windows, then obtaining the inverse transform of their product.

4.3 Fold of a Rectangle into a Gaussian Curve

$$\text{Let } f_s(x) = \begin{cases} 1 \text{ when } |x| < d \\ 0 \text{ when } |x| \geq d \end{cases}$$

a rectangular window, and let

$$f_c = \frac{h}{\sqrt{\pi}}\, e^{-h^2x^2} \qquad (5)$$

be a Gaussian curve. The normalization is such that the rectangle is of unit height and the area under the Gaussian is 1. Using eq. (2)

we find, using [10] Dw. 863.3 that

$$\bar{f}_s(s) = \frac{1}{\sqrt{\pi}} \frac{\sin ds}{s}, \quad \bar{f}_c(s) = \frac{1}{\sqrt{2\pi}} \exp\left(-\frac{s^2}{4h^2}\right) \quad (6)$$

Using eq. (4) and eq. (5), the line profile becomes

$$f_p(x) = \frac{2}{\pi} \left[\operatorname{erf} h(d+x) + \operatorname{erf} h(d-x)\right] \quad (7)$$

The integration makes use of Dwight[10] 863.3 . The error function erf u is defined in[10] Dwight 590.

4.4 Fold of an Exponential Window into a Gaussian Window

Let us now consider an exponential window,

$$f_s = \begin{cases} 0 & , \ x < 0 \\ e^{-ax} & , \ x \geq 0 \end{cases}$$

such as might be encountered in a tapered slit through whose edge radiation penetrates. We wish to fold this function into the Gaussian of eq. (5). Using the formalism described above, the line profile becomes

$$f_p(x) = \frac{1}{2} \exp\left(-ax + \frac{a^2}{4h^2}\right) \left[1 + \operatorname{erf}\left(hx - \frac{a}{2h}\right)\right] \quad (8)$$

4.5 Line Profile for a Slit

Consider a hypothetical slit of the general type shown in fig. 8 with an open gap of width 2d, and suppose for the moment that the absorption in the cheeks is such that the slit window is given by (fig. 11)

$$f_s = \begin{cases} 1 & , \ |x| \leq d \\ e^{-a(|x| - d)} & , \ |x| > d \end{cases}$$

The profile can be calculated from the profiles due to a rectangular window and due to an exponential window, for by superposition we may add the effects of three regions. The effect of region II is given in eq. (7). The effect of region I is given by replacing x by x-d in eq. (8). That of region III is given by replacing x by -x-d in eq. (8). The resulting profile is

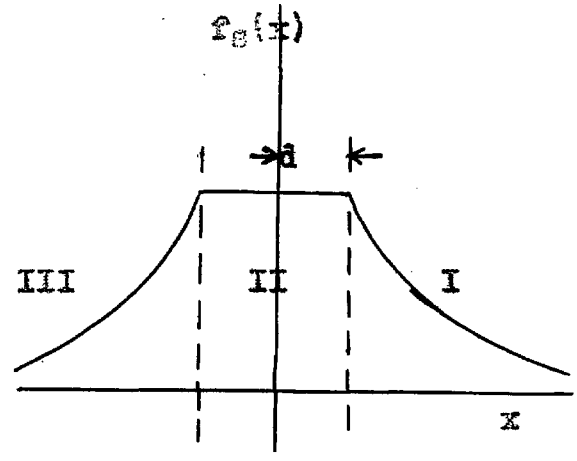

Fig. 11 Hypothetical slit window

$$f_p(x) = \frac{2}{\pi}\left[\operatorname{erf} h(d+x) + \operatorname{erf} h(d-x)\right] +$$

$$+ \frac{1}{2}\exp\left[a(d+x) + \frac{a^2}{4h^2}\right]\left\{1-\operatorname{erf}\left[h(d+x) + \frac{a}{2h}\right]\right\} +$$

$$+ \frac{1}{2}\exp\left[a(d-x) + \frac{a^2}{4h^2}\right]\left\{1-\operatorname{erf}\left[h(d-x) + \frac{a}{2h}\right]\right\} \quad \text{eq. (9)}$$

Evidently, if we define the function

$$g(u) = \frac{2}{\pi}\operatorname{erf} hu + \frac{1}{2}\exp\left[au + \frac{a^2}{4h^2}\right]\left\{1 - \operatorname{erf}\left[hu + \frac{a}{2h}\right]\right\} \quad \text{eq. (10)}$$

then $f_p(x) = g(d+x) + g(d-x)$ eq. (11)

In some cases it becomes necessary to study the effect on the line profile of variation of d. The fact that g(u) is independent of d makes it possible to make quick plots of f_p with various values of d. It is merely necessary to make a single plot of g(u), and a tracing. By turning over the tracing, superposing the coordinate axes of the two curves, then sliding the tracing to the right through a distance corresponding to 2d, we have then superposed, with appropriate

axes, g(d+x) and g(d-x). It is easy to add two such curves with dividers, and there results the line profile corresponding to the gap 2d. This is an illustration of a technique which can be applied regardless of the form of the function representing the absorption in the cheeks, as long as the slit is symmetrical. In some cases numerical integration would be necessary in order to find g(u), but once it is determined, the variation with d can be quickly found. g(u) can thus be regarded as a kind of generating function corresponding to a given slit at a certain energy.

4.6 The Line Profile of the Slit for 2.62 MeV Radiation

In order to calculate in an approximate way the line profile of 2.62 MeV radiation of ThC''-D in the Hevimet source holder (fig. 8), the approximations were made that the jaws are infinite in length in the beam direction and that the source itself is of uniform intensity in the direction of the beam. The source window takes the following form (all lengths have been referred to the focal circle):

$$f_s(x) = \begin{cases} 2\beta, & |x| \leq d \\ \displaystyle\int_0^\infty \frac{\exp\left\{\frac{-2\mu(|x|-d)(u+1)}{1.18\beta}\right\}}{u^{1/2}(u+1)^{3/2}}\,du, & |x| > d \end{cases} \quad \text{eq. (12)}$$

where 2β is the angle of divergence of the beam, 2d is the gap, μ the absorption coefficient, and u is a variable of integration which varies with the angle of the ray passing through the slit, all measured in millimeters where appropriate.

This expression is difficult to integrate and probably would result in additional difficulty in Fourier transformation. For the present purpose it is considered sufficient to approximate the integral

by an "average" exponential function. The function so chosen is $\exp\left[-\frac{5\mu}{\beta}(|x| - d)\right]$ for $|x| > d$, for it has approximately the same 1/e value as the integral. Setting $a = \frac{5\mu}{\beta}$ in eq. (10), the generating function was computed from the constants of the problem and is shown in figure 12.

Since the height of the line is proportional to 2g(d) (see eq. 11 with x = 0), it is possible to find an optimum value of d for searching for the 2.62 MeV line. We know that the line will certainly be wide compared to the interval between points on the wavelength scale, as we scan the line. Hence we may assume that the best chance of finding this weak line occurs when the ratio of peak to background is a maximum. Since the background in this short-wavelength region is almost proportional to the strength of the beam, the problem simplifies to that of finding the value of d which results in the highest ratio of line-profile height to source window area. From the constants of the problem, the source window area is given by 0.11 + 2d (the source window is of unit height). A simple graphical analysis gives a broad maximum of this ratio near 2d = 0.08. Referring this to the focal circle gives 0.068 mm for the best width of the source, with wide limits because of the broad maximum. This value was used in the search for the 2.62 MeV line, with negative results however.

There is plotted also the g(u) (in this case an error function) corresponding to the rectangular window. This curve has been used to obtain the line profile for the 238 KeV line γ-ray of ThB-C, with 2d = 0.125 mm since the cheeks are so absorbing that only the

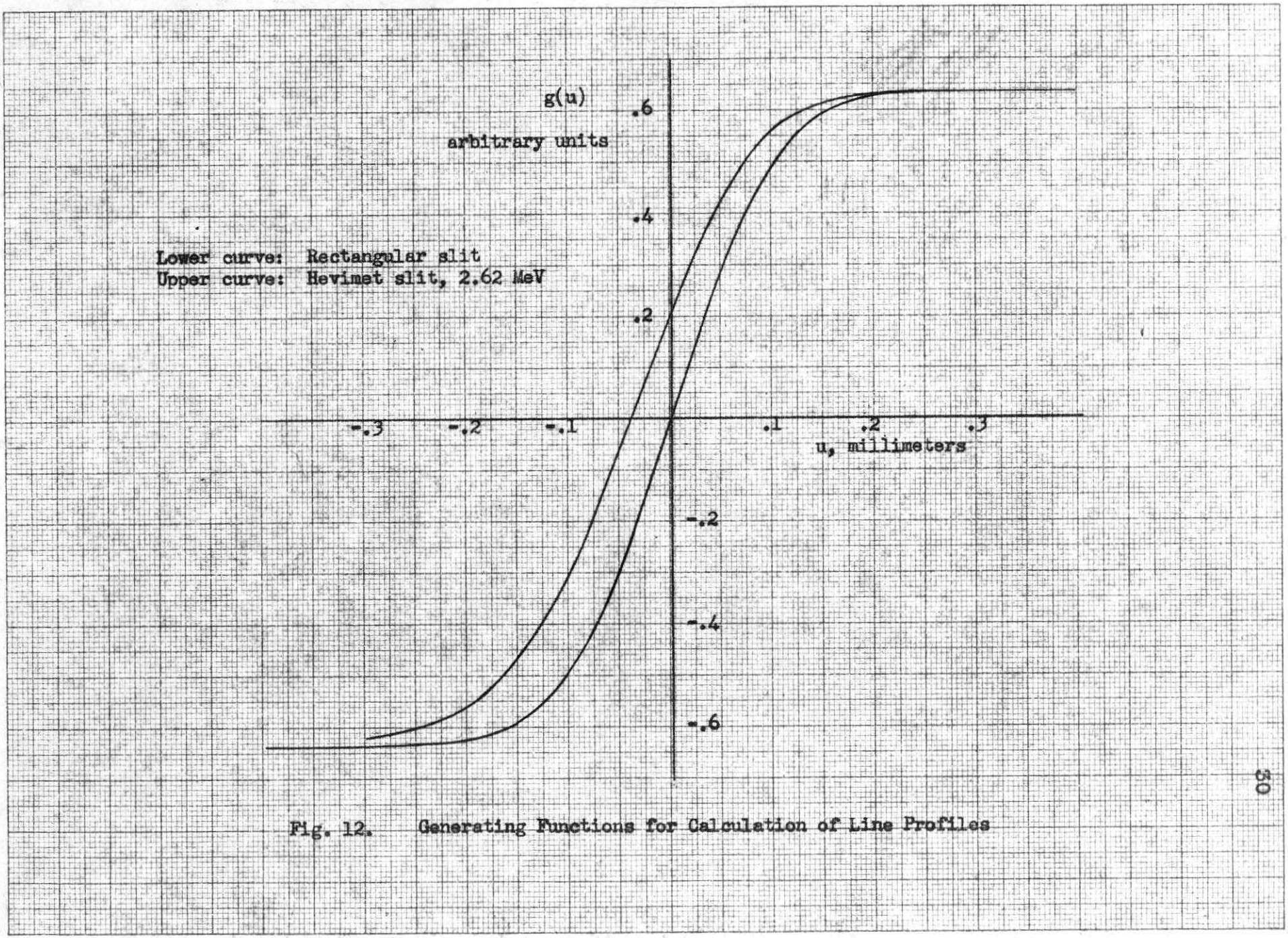

Fig. 12. Generating Functions for Calculation of Line Profiles

gap is important. The observed width agrees well with the calculated width (fig. 15).

4.7 Radon Line Profiles

One source of Rn in the flattened tube displayed a steeple-like line profile (fig. 14). This is thought to result in some way from the peculiar distribution of active deposit in the tube (fig. 5). Since most of the active deposit is on the flattened sides of the tube, the source window approximates two δ-functions separated by a distance $2d = 0.16$ mm. Inserting appropriate functions in eq. (1) gives

$$f_p(x) = \frac{h}{\sqrt{\pi}} \int_{-\infty}^{\infty} \left[\delta(z-d) + \delta(z+d)\right] \exp\left[-h^2(z+x)^2\right] dz$$

$$= \frac{h}{\sqrt{\pi}} \exp\left\{-h^2(x+d)^2\right\} + \frac{h}{\sqrt{\pi}} \exp\left\{-h^2(x-d)\right\}, \quad \text{eq. (13)}$$

the sum of two Gaussian curves displaced from each other. Approximately one-quarter of the activity of the source, however, is on the rounded front and rear sides, and this portion would be expected to produce a more peaked type of profile. The peaks of the Gaussians would be expected to give rise to the bends in the sides of the line profile. Thus the main features of the line profile are thought to be explained, at least qualitatively, by the source makeup.

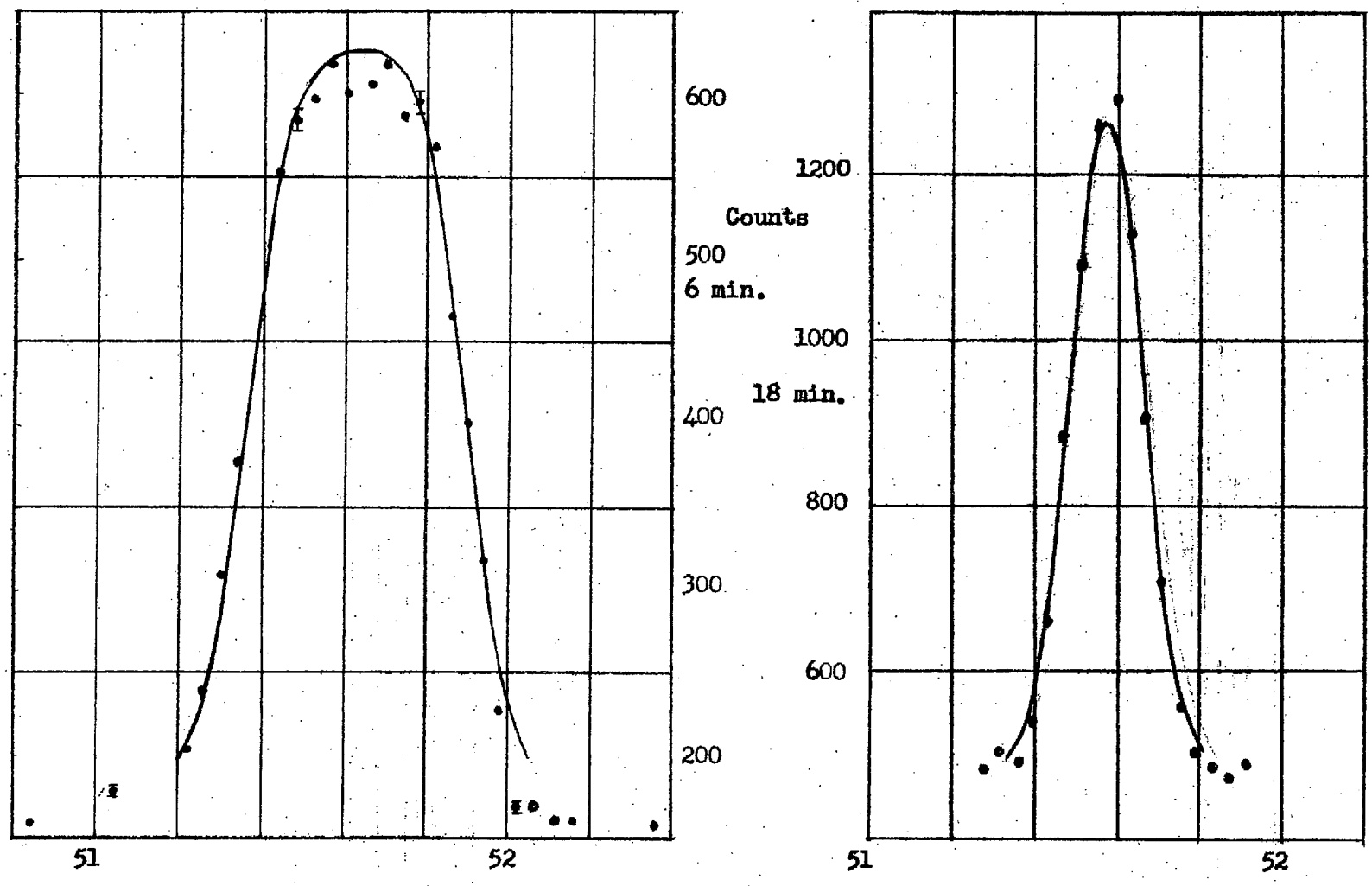

Fig. 13. Line profile of the 238 kev line of ThB-C. At the left, a lead source holder was used, for which the source capsule was too large. The solid line shows a properly normalized curve, calculated by the method described, for the resulting 0.43 mm (abnormally large) gap. At the right, the Hevimet holder was used with 0.1 mm gap, and the solid line is the calculated profile. A scale of 16 was used in counting.

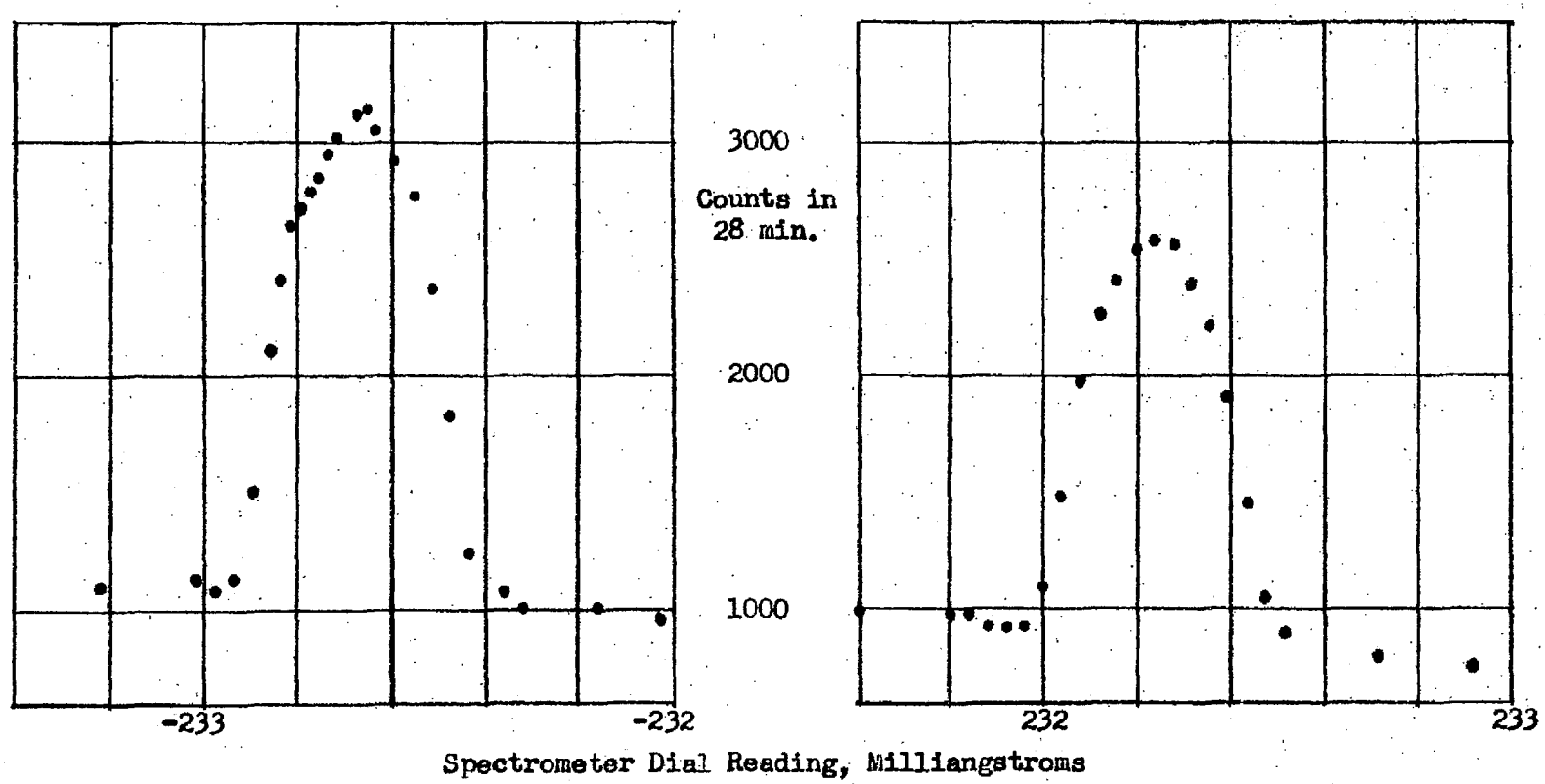

Fig. 14. Unrefined data on 52.8 kev line of RaB-C. The effect of source decay is seen in the sloping background and in the lower peak on the positive side of the instrument. A scale of 16 is used in counting.

V

THE RADIATION DETECTOR

Development of a suitable radiation detector for use with the curved-crystal spectrometer was one of the most exacting problems to be encountered in connection with the instrument. The following properties are essential in such a radiation detector:

(1) High efficiency to gamma radiation.

(2) The detector must be of such a size that it will accept the entire diffracted beam, thus making use of the entire area of the quartz crystal.

(3) Small volume, consistent with this large area to the beam, is desirable in order to reduce the sensitivity of the counter to background radiation.

(4) Spurious effects must be kept at a minimum, in order to insure that the statistical precision of counting is limited only by the number of counts registered during a measurement.

The following three types of radiation detectors have been considered:

(a) Geiger counters

(b) Proportional counters

(c) Scintillation counters

5.1 The Original Gas-filled Counters

The original multicellular Geiger counters for this instrument were developed by Lind[11]. Enclosed in a round steel tube of 3"

inside diameter were from six to ten coaxial plates of cathode material, usually lead, spaced 5/8". Interposed between these plates were the anode structures, supported on a central rod. These structures consisted of four tungsten wires of 10 mil diameter arranged in a cross in order to give good coverage of the space between the plates, and whose four free ends were coated with glass beads to avoid high field.

These counters were 10% efficient at 1.2 MeV, as measured by coincidence methods using the gamma radiation of Co^{60} (see p. 46). They had the disadvantage of short life, a few months at most, and frequently required complete disassembly and overhaul.

5.2 Four-wire Counters of Square Cross-section

The construction of a new and larger collimator[12] made it profitable to increase the area of the detector to 3" x 3", as presented to the diffracted beam. New counter envelopes were constructed of square tubing 3" in inside dimension and 8" long (fig. 15). Counters were designed using square plates lying in planes normal to the axis, and bearing 3/8" holes arranged on a 1 1/2" square. After the plates had been inserted, with 1/4" thick square spacing rings, the four anode wires of 2 mil tungsten were strung through the holes.

A great deal of difficulty was experienced with this type of counter in attempts to make it work satisfactorily. These attempts were continued because in each attempt it was possible to show some counting character in the tube. The undesirable symptoms were of

two types; either the tube showed many spurious* counts immediately after filling, which usually meant that a spark discharge was taking place, or, as was more frequent, the tube showed a good characteristic soon after filling (when proper mixing of the gases had taken place), with a counting range of about 100 volts, but after one day of lying idle, the discharge voltage (the high-voltage end of the counting range) would begin to creep down, swallowing up the plateau, until after a few days the counter would simply go into discharge immediately after beginning to count (fig. 16).

The effect of cathode materials was tested using solid plates of five different materials, Bi, Pb, Cu, Ag, and Ta. The only successful counter thus made was with Cu plates. The other materials were uniformly unseccessful, with Bi perhaps worse than the rest. Counters with Bi (75% Bi and 25% Pb) appeared to spark or discharge more readily than was usual with other materials. It was possible to electroplate Cu on the plates of Bi, of Pb, and of Ta. This was done, but no certain improvement resulted.

---

* Spurious counts made themselves evident on the oscilloscope screen, where they appeared as groups containing a large or a small number of counts, which were presumed to follow a bona fide count. Individual spurious counts could be recognized if they followed the main count so closely that the counter or the circuit did not have time to recover completely. In this case they were not of full height. Some of the possible causes of spurious counts will be explained.

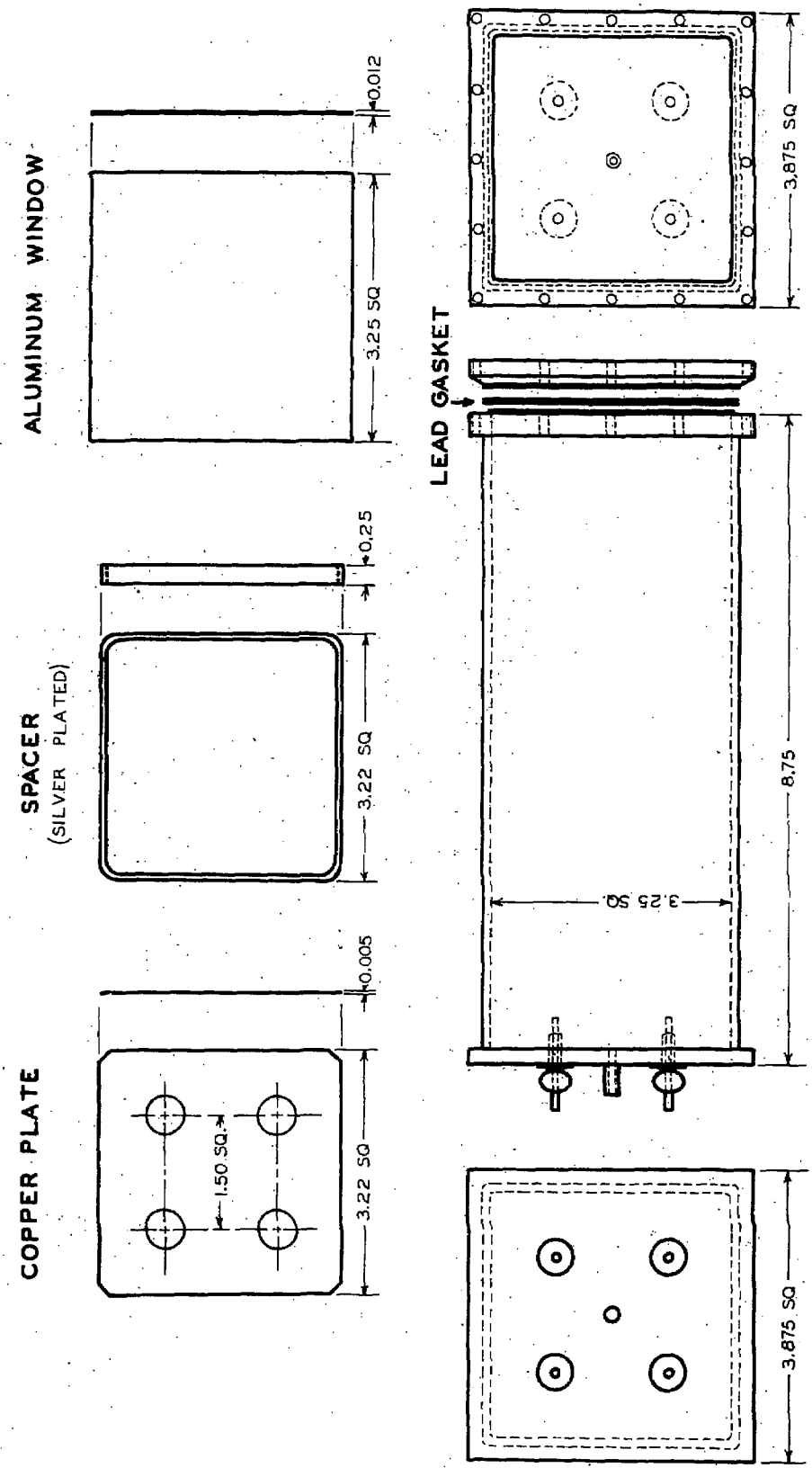
ALUMINUM WINDOW
0.012
3.25 SQ
SPACER
(SILVER PLATED)
0.25
3.22 SQ
COPPER PLATE
0.005
1.50 SQ.
3.22 SQ
LEAD GASKET
3.875 SQ
3.25 SQ
8.75
3.875 SQ
COUNTER CASE

FIG 15

The plates were prepared by careful cleaning with steelwool, nitric or hydrochloric acid, and rinsings in distilled water and acetone. In some cases they were treated in a degreaser using carbon tetrachloride, in which the solvent collected on the plates and dripped off. The final rinse was usually clean acetone, and the plate was warmed while it was drying in order to avoid the condensing of moisture and subsequent oxidation of spots on its surface. In some cases the plates of Cu, Ag, or Ta were baked in H_2 at 300° C, and in vacuo at 600° to 750°, then installed immediately. In all cases they were inspected carefully on assembly to make certain that they were free of dust and other foreign matter, as were all other internal parts of the counters.

Anode wires were of W, in most cases .002 inches in diameter. The four anodes were arranged in pairs, with each pair consisting of a single wire. The wire was soldered into a Kovar insulated bushing in the rear of the counter case (fig. 15), traveled through one set of holes to the front of the counter, traveled over two glass rods to an adjacent set of holes, thence through this second set of holes to another Kovar bushing in the rear of the counter. Since the two ends of each wire were brought to connections outside of the case it was possible to glow the wires in order to burn off dust and impurities. By this process it was shown that several times the anodes were at fault, for glowing them restored the counter to temporary operation.

In a few cases, glass beads were placed on the anode wires at 2 inch intervals in order to halt the spread of the discharge, with the hope that deterioration of the quench gas and deterioration or excitation of the cathode surfaces would be minimized. These

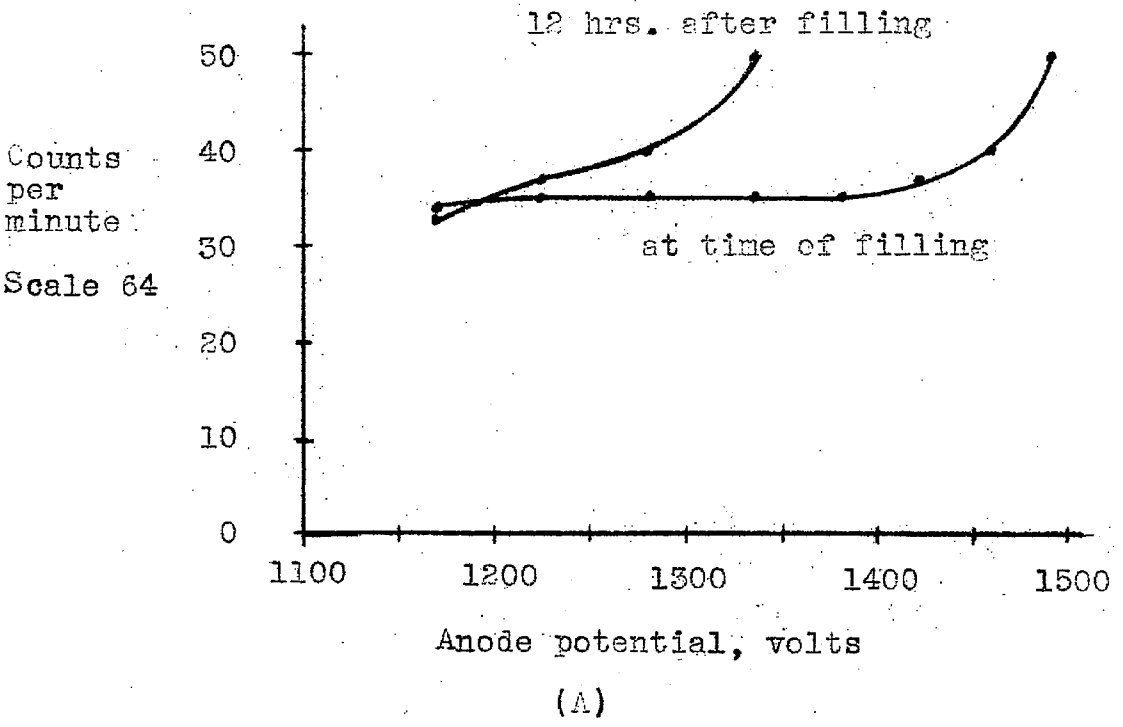

(A)

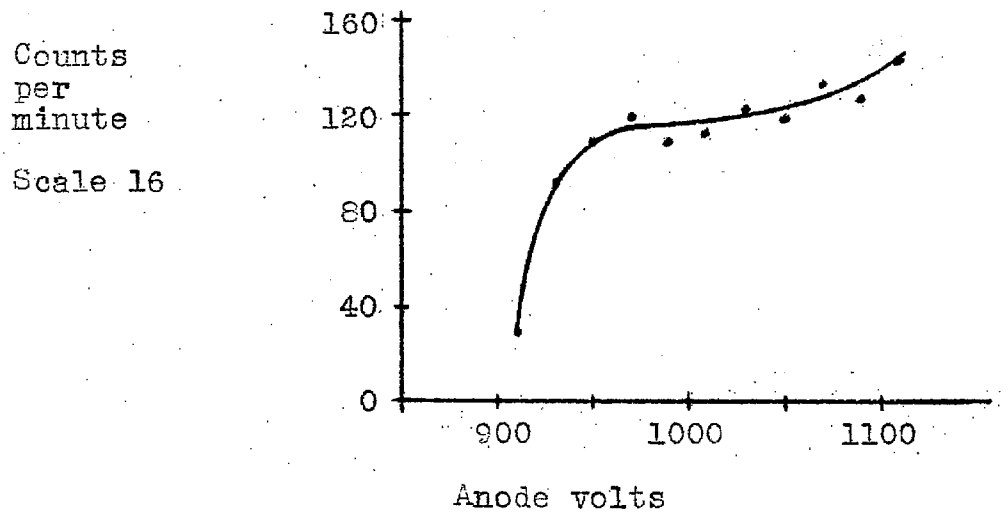

(B)

Fig. 16. Characteristics of two types of Geiger counters of square cross-section. (A) Typical characteristic of straight-wire counter. (B) Characteristic of circular-anode counter.

attempts failed; the counter showed no Geiger action, only discharge.

Several precautions were found to be necessary in order to avoid sparking and leakage of the high voltage, in addition to the elimination of dust and other foreign particles already mentioned. The insulating bushings (manufactured by Stupakoff) were cleaned with acetone both before and after their assembly into the cases. They have been known to show leakage when this is not done, and this leakage shows up as "grass" on the oscilloscope screen. As another precaution, the holes in the cathode plates were carefully polished after they were punched, and the edges were rounded. In the case of thin plates, .005" and thinner, they were actually flanged, so that the sharp edge pointed in a direction normal to the plate rather than directly toward the wire. In some cases of persistent sparking, or where many spurious counts appeared in the counting range, the holes were enlarged to 1/2" diameter. The one successful counter had 1/2" holes.

A great variety of mixtures of gases were tested. In all cases, argon was used as the principal component, and various quench gases were used. Petroleum ether, alcohol and ethylene exhibited much the same properties. A great change in the behavior of the counter resulted from the addition of a small amount of ethylene dibromide. This compound has the property of absorbing free electrons, and by so absorbing electrons in the regions of weak field within the counter it was able to diminish the counting rate by a factor of about ten. Even after the mixture was pumped out and replaced, the small trace of ethylene dibromide remaining in the counter had effect, and the counting rate was one-third the normal counting rate. It was not

possible to find a concentration of this substance which would eliminate spurious counts without a radical reduction in sensitivity.

Operation of the counter was a strong, but not critical, function of the total pressure of gas and the percentage quench gas, but it was seldom difficult to find a combination which would work. With a .002 inch diameter anode wire, representative filling mixtures are 5% ehtylene or petroleum ether in argon, total pressure 34 cm Hg, and 3% ethylene in argon, total pressure 50 cm Hg. Other combinations were tested, ranging in total pressure from 10 cm to 75 cm Hg and in quench concentration from 2% to 15%.

A large number of theories were advanced in explanation of our difficulties, and very few have survived examination by experiment. It is known that regions of weak field in the counter can accumulate free electrons and negative ions during the Geiger discharge, and these electrons can subsequently drift into stronger portions of the field to cause delayed counts. On the other hand, regions of the cathode at which the field is large can exhibit the so-called Paetow effect[13], which is thought to result from excitation of the cathode surface by photons from the anode avalanche, and subsequent release of an electron from the cathode, to cause a delayed count. This results in an excitation of the counter at high counting rates, which we observed by reducing the voltage to normal operating value after spark or glow discharge, and observing that the counting rate reduced only very slowly, in a matter of a minute. If, now, the geometry of the counter is extremely radical, that is, if the field takes on very high values and very low values at different parts of the

cathode, it may be impossible to find such a quenching mixture that the cathode will be quenched for a suitable anode operating voltage, while at the same time all parts of the gas volume will have sufficient field to clear out stray electrons.

It was, as a matter of fact, possible to build a lasting counter using the same parts, provided that the geometry was modified to a less radical geometry. This tends to vindicate the methods used in the construction and preparation of parts for the counters, but does not explain why one of the four-wire tubes (in contrast to six unsuccessful but apparently identical other attempts) performed satisfactorily for many months.

5.5 Square Counters with Circular Anodes

In order to recreate the conditions of the 4-prong anode parallel plate counter, which had known some success, anode structures were made in the shape of circular loops of 4 mil tunsten wire, and supported by rods passing through holes in the cathode plates. With the exception of the anodes, the same parts were used to construct these counters, three of which were assembled. Plate spacings of 1/2", 5/8", and 1/4" were used. With small plate spacing it becomes difficult to hold the geometrical tolerances closely enough to avoid sparking between a portion of the anode and the cathode, and to make the plateaux of the individual sections overlap to the extent that they can all operate at the same applied voltage. With reasonable care, it was possible to assemble a counter of ten cells, which exhibited a plateau of about 100 volts (fig. 16) with a filling mixture of 30 cm total pressure, argon and 5% petroleum ether. This counter was never used

in the spectrometer however, due to the development of the scintillation counter.

5.4 Use of the Multicellular Counter in the Spectrometer

In operation, the multicellular counter was placed in an assembly such that it was surrounded by fourteen Geiger counters and the entire assembly was supported behind the collimator and surrounded with 4" of lead for shielding against gamma ray background. The fourteen counters which surrounded the main counters and which were intended to reduce the background counting rate due to penetrating cosmic ray particles, were connected in anti-coincidence with the main counter so that an event which actuated one or more of the protective ("anti-coincidence") counters would not be registered in the scalar, even if the main counter were simultaneously actuated by the event.

A block diagram of the electronic circuitry is shown in figure 17. The provision for combining the signals from the main and anti-coincidence counters is indicated. Multivibrator quench circuits were provided for all counters in order to preserve their life, to give a flatter counting characteristic, and to form reliable pulses which could be used in the anti-coincidence and scaling circuits. The high voltage and power supplies were regulated in order to minimize changes in the sensitivity of the counters and in the operation of the circuits due to line voltage changes. For the purpose of automatic operation, the scaler operated a printing register in the robot observing mechanism.

5.5 The Efficiency of Multicellular Counter Tubes for Gamma Rays

The efficiency of a gamma-ray counter with thick converter walls has been shown[19] to be equal to the sum of three terms, corresponding to the photoelectric effect, Compton effect, and pair production.

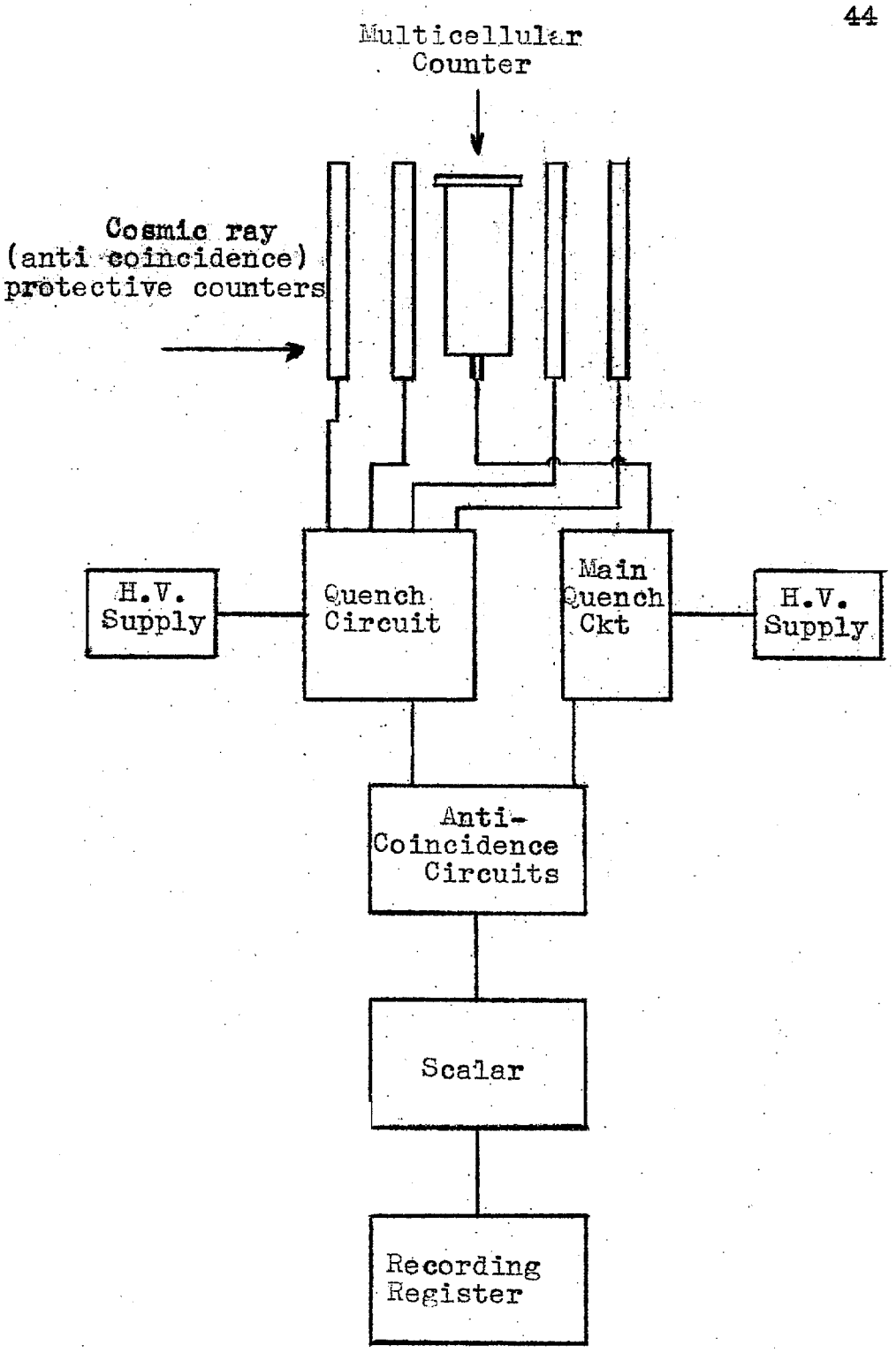

Fig. 17 Block diagram of Geiger counter detector. Each of the four sides of the main counter is protected by a bank of three or four protective counters connected in parallel. Each such bank has an input to the large quench circuit.

Often one or two of these terms will be negligible compared to the third. In each case, the term is proportional to the product of the absorption coefficient for the process to the radiation, and the range of the electron secondaries. If the effective range of the secondaries is greater than the thickness of the plates, then the range is to be replaced by the thickness in the expression.

For each process, the efficiency is an increasing function of Z. In the case of the photoelectric process it is proportional to Z^4, disregarding absorption edges, while in the case of Compton conversion it is a slow function resulting from a logarithmic factor in the electron energy loss by collision[15]. For pair production the efficiency should be proportional to Z. The increase of efficiency with Z is confirmed by experiments[16] and it is for this reason that we attempted to make plates of elements of high Z.

The efficiency of a counter of a given material is greatest at a given energy if the plate is made of thickness equal to the range of the secondaries of the predominant process, provided that the gamma-ray absorption is small in this thickness. However, when a number of such plates are placed in tandem, the last plates have less radiation than the first because of the attenuation of the preceding plates. By reducing the thickness of the plates by a calculated amount it should be possible to increase the efficiency of the counter by giving a more equitable distribution of radiation along the length of the counter. This was done in some of the later counters designed for certain energy ranges, but as has been mentioned, it was impossible to make these particular counters work satisfactorily.

It is of interest to carry out a calculation of the efficiency of a gamma-ray counter and to compare the result with that which can be observed. Let us consider a counter using 10 plates of Pb .05 cm in thickness, measuring gamma radiation from Co^{60}, which can be considered to be of energy 1.2 MeV. If we wish to assume that all the secondaries travel forward, we find that since the range is about .08 cm and the absorption coefficient 1.2 cm^{-1}, all of the secondaries should get out, and the efficiency per plate is

$$\epsilon_o = (1.2) \times (.05) = .06.$$

The effect of 10 plates, if the absorption of the beam by the plates is taken into account, is to multiply this efficiency by 7.7, and the resulting overall efficiency would be 46%.

The assumption that all the electron secondaries get into the sensitive volume is, however, highly optimistic. In fact, curves of Geiger counter efficiency[17] indicate that a counter with a thick Pt cathode should have an efficiency of 1.4% at this energy. If we assume that Pb with thinner walls and higher Z, has the same efficiency, the total efficiency for 10 plates will be only 10.8%.

A measurement was made of the absolute efficiency of this counter using Co^{60} radiation. This radiation consists of one 1.1 MeV gamma ray and one 1.3 MeV gamma ray for every disintegration, in coincidence. The specific activity of a Co^{60} sample is so high that the self-absorption is negligible. Also there is very little or no direction correlation between the two gamma rays. They are therefore taken as two 1.2 MeV gamma rays with no absorption or correlation

but in perfect coincidence.

For this measurement two counters were used (fig. 18). One was the counter of 10 cells with 4-prong anodes and Pb plates, described above; the other was of 6 cells, the plates consisting of 100 mesh brass wire gauze plated with about 0.05 cm of Ag. The two counters were shielded with 2" of Pb and the Pb-plate counter was protected with cosmic ray anticoincidence counters. In the position shown in the figure, measurements are made of the individual counting rates and of the coincidence rate. If we assume all of the counting to be genuine and due only to the Co^{60} source, and if we label the Pb-plate counter #1, letting N_1, N_2, and N_{12} be the individual counting rates and the coincidence rate, and S the (unknown) strength of the source in disintegrations per second, we may write

$$N_1 = S\sigma_1, \qquad N_2 = S\sigma_2 \qquad \text{eq. (1)}$$

where σ_1 is the probability (proportional to solid angle and to efficiency) of counter #1 registering an arbitrary gamma ray from the source, and similarly with σ_2. With no angular correlation between the gamma rays, we can write the probability per unit time of both counters registering the rays of a single disintegration,

$$N_{12} = (S\sigma_1)\ \sigma_2 \qquad \text{eq. (2)}$$

Eliminating σ_1, σ_2 from these two expressions results in

$$S = \frac{N_1 N_2}{N_{12}} \qquad \text{eq. (3)}$$

Knowing S, we can find the efficiencies of the two counters by counting with this source at a large distance r and applying eq. (1) with

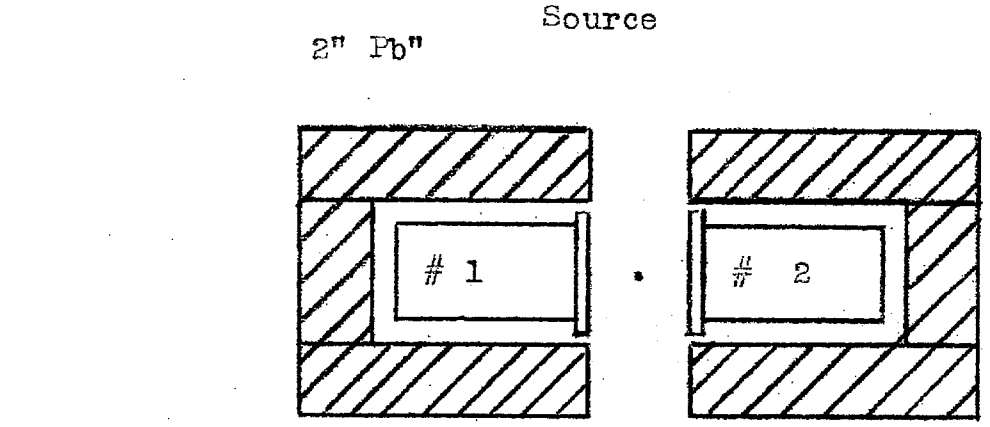

A

B

Fig. 18 Experimental setups to measure absolute efficiencies of gamma ray counters; (A) setup for measurement of absolute source strength, (B) setup for measurement of counter efficiency.

$$\sigma_1 = \frac{(\text{area of counter}) \times \epsilon_1}{4\pi r^2} \qquad \text{eq. (4)}$$

here ϵ_1 is the efficiency, which we can now find.

In the application of this method, the individual counting rates must be corrected for dead time and for background counting rate, and the observed N_{12} must be corrected for accidental coincidences and for a background coincidence rate, probably due to cosmic ray showers and the like.

This experiment yielded an efficiency for the Pb-plate counter of 10.2%, and for the Ag plated counter of about 5%. Thus it is evident that attempts to calculate efficiencies of gamma ray counters are difficult, requiring more knowledge of the behavior of secondary electrons than is readily available.

5.6 A Check of Counting Statistics

It has been mentioned above that one of the necessary properties of a photon counter is that of good statistics of counting. This necessitates freedom from spurious counts, and constancy of sensitivity with time. A very sensitive test of this property is provided in the "chi-squared" test[18]. For this test, the total count is measured a number of times for a given time interval and with a constant source. Different observed values will, of course, be recorded for these different trials, due to the randomness of distribution of the pulses. From these observed values a quantity χ^2 is calculated. The function $g(\chi^2)$, listed in tables, gives the chance of observing this value or a greater value of χ^2 if the distribution of counter pulses were perfectly normal. Let x_i be the i^{th} measurement of the count, in individual pulses, where N such trials are made. If x

is the expected value of the count, which can here be taken as the arithmetic mean of the N observations, the value of chi-squared is defined to be

$$\chi^2 = \sum_1^N \frac{(x_i - x)^2}{x}$$

The function $g(\chi^2)$ is found by entering the table with the value of χ^2 and the number of degrees of freedom. The number of degrees of freedom is here taken to be N - 1, because the N numbers x_i, rather than being independent, are connected by the single averaging relation,

$$\sum_1^N x_i = N\,x$$

As an example of the application of this test to a Geiger counter, let us examine a portion of the spectrometer search for the low energy lines of Ta^{182}, which was conducted by J. R. Brown[19] using the counter with 5 mil copper plates. The data appear in the following table:

DATA OBSERVED FOR THE PURPOSE OF A CHI-SQUARED TEST OF A COUNTER

Screw Setting	Observed Count $x_i/16$	Nominal Deviation $(x_i-115)/16$	$(x_i-115)^2/16^2$
51.52	113	-2	4
.56	119	4	16
.60	119	4	16
.64	114	-1	1
.68	119	4	16
.72	114	-1	1
.76	116	1	1
.80	112	-3	9
.84	112	-3	9
.88	117	2	4
.92	119	4	16
.96	122	7	49
52.00	117	2	4
.04	117	2	4
.08	114	-1	1

DATA OBSERVED FOR THE PURPOSE OF A CHI-SQUARED TEST OF A COUNTER (Cont.)

Screw Setting	Observed Count $x_i/16$	Nominal Deviation $(x_i-115)/16$	$(x_i-115)^2/16^2$
52.12	119	4	16
Sum			167
Average	116.44	1.44	

Since no line appeared in this region of search, it is reasonable to assume that the counting rate should have remained constant. The nominal deviation was obtained by subtracting 115 in order to facilitate use of a device for obtaining the sum of the squares of the deviations in a simple manner. This becomes

$$\sum_1^{16} (x_i - 116.44)^2 = \sum_1^{16} (x_i - 115)^2 - 16(115 - 116.44)^2 = 134$$

Since the counting has been scaled down by a factor of 16, this factor must be introduced in the numerator in order to assure that individual counts have been considered, for scaled-down counts cannot be expected to follow a normal distribution. We obtain

$$\chi^2 = \frac{16 \cdot 134}{116.44} = 18.4$$

Entering a table of the χ^2 distribution[18], we obtain, for 15 degrees of freedom, $g(\chi^2) = 0.245$. A test on an adjoining region gave $g(\chi^2) = 0.533$. In the former case, this means that this run shows greater deviation than about 75% of similar runs (same counting rate and same number of samplings) using a perfectly random counter, so no definite information is furnished by this test as to the randomness of counting.

The randomness of counting in this instance is limited by the fact that the scalar rounds off the total count to the nearest 16, since only the register counts can be printed. Counts stored in the scaling circuit (lights) are dropped if they are less than 8 in number, and a register count is added if they are 8 or more in number. It can be easily shown that the r.m.s. error introduced by such resettings is 0.214 register counts. In order to obtain a feeling for their possible effect on the above test, note that the standard deviation to be expected for a total of 116.44 register counts is 2.7, and since the error introduced by resetting should add in quadrature, the effect on the value of χ^2 will be negligible.

In order to see how sensitive this test is to spurious counts, we may note that a 35% increase in χ^2 would result in a reduction of $g(\chi^2)$ to about 0.06. This might be expected if the experiment were to be repeated with the counter in such a condition that one-third the bona-fide counts were accompanied by single spurious counts. The conclusion is that the copper-plate Geiger counter displays good statistics, so that its true efficiency is not appreciably impaired by this consideration.

5.7 Proportional Counters

Use of the counters in the proportional region was contemplated for a time, and was proposed in the hope that this mode of operation would increase the life of the counter, since the quenching action in the Geiger region is supposed to destroy quench gas and to poison the cathode surfaces. Accordingly one of the 4-prong anode counters mentioned above was connected as a proportional counter using a

Jordon-Bell amplifier and cathode follower preamplifier, and the pulse height spectrum was studied. This spectrum showed a predominance of pulses of low voltage which merged with the noise spectrum of the amplifier (fig. 19). This was interpreted as resulting from the fact that of the electrons emitted from the cathode-converter plates of the counter, those of low energy predominate, as would be expected in the case of Compton scattering, and a large number of gamma-ray electron conversions in the counter result in voltage pulses too small to be detected whereas their electrons would have caused Geiger counts. This fear was confirmed by the fact that for the background radiation in the laboratory, the same counter acting as a Geiger counter had a much higher counting rate than as a proportional counter with the pulse height discriminator set to the top of the noise spectrum. In the case of a counter in which conversion takes place in the gas, for instance the xenon-filled counter used by G. L. Felt[20] in recent measurements of h/e, this loss of efficiency should not occur, for there are no plates in which to slow large numbers of secondaries to the point where they cannot cause counts larger than noise.

It was concluded that the use of proportional counters at nuclear energies would introduce such a loss of efficiency or decrease of stability (because of a possibly unstable discriminator separating noise from pulses) that it was not a suitable detector for the curved crystal spectrometer.

5.8 The Scintillation Counter

The most satisfactory answer to the detector problem appears to lie in the scintillation counter in present use with the instrument.

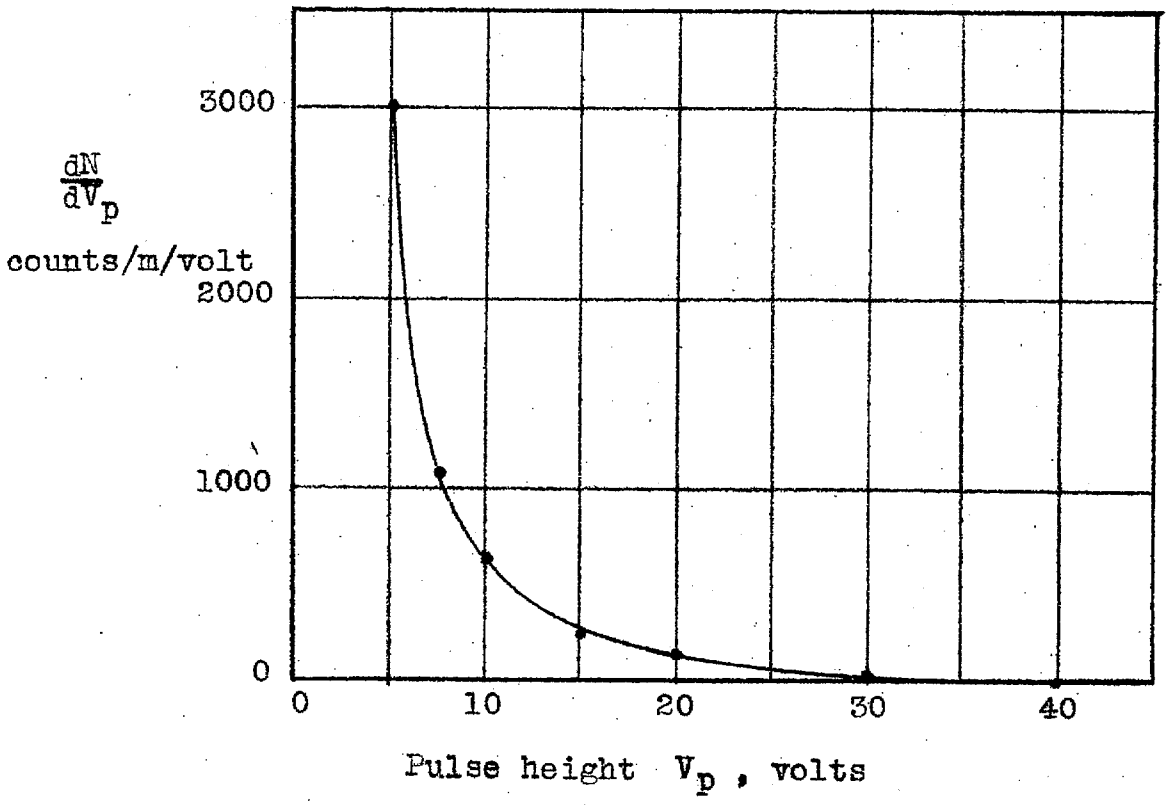

Fig. 19 Differential pulse height spectrum of the proportional counter

A block diagram of the scintillation detector is shown in figure 20. The following features are provided:

(1) The scintillating phosphor is a crystal of thallium activated sodium iodide, a dense material of fairly high atomic number, providing high absorption to nuclear gamma radiation.

(2) Two phototubes must simultaneously respond to a light pulse within the crystal in order for the pulse to be recorded. This reduces the response to phototube noise to a negligible value since such noise pulses are not in coincidence.

(3) Pulse height discriminators are provided, which allow pulses of an adjustable band of heights to be recorded. By this means it is possible to eliminate large pulses, such as those due to penetrating cosmic ray particles and background radiation of high energy, and to eliminate very small pulses, as those due to accidental coincidence of noise pulses in the two phototubes or low energy background radiation.

(4) The scalar is so wired that it works in conjunction with the automatic observing mechanism.

For a more complete description of the design and operation of the scintillation detector, see reference 21.

In efficiency, the scintillation detector promises to be from three to seven times better than Geiger counters, depending on the energy of the radiation to be measured. It has indefinite lifetime and is more reproducible than a Geiger counter. It can operate over a wide

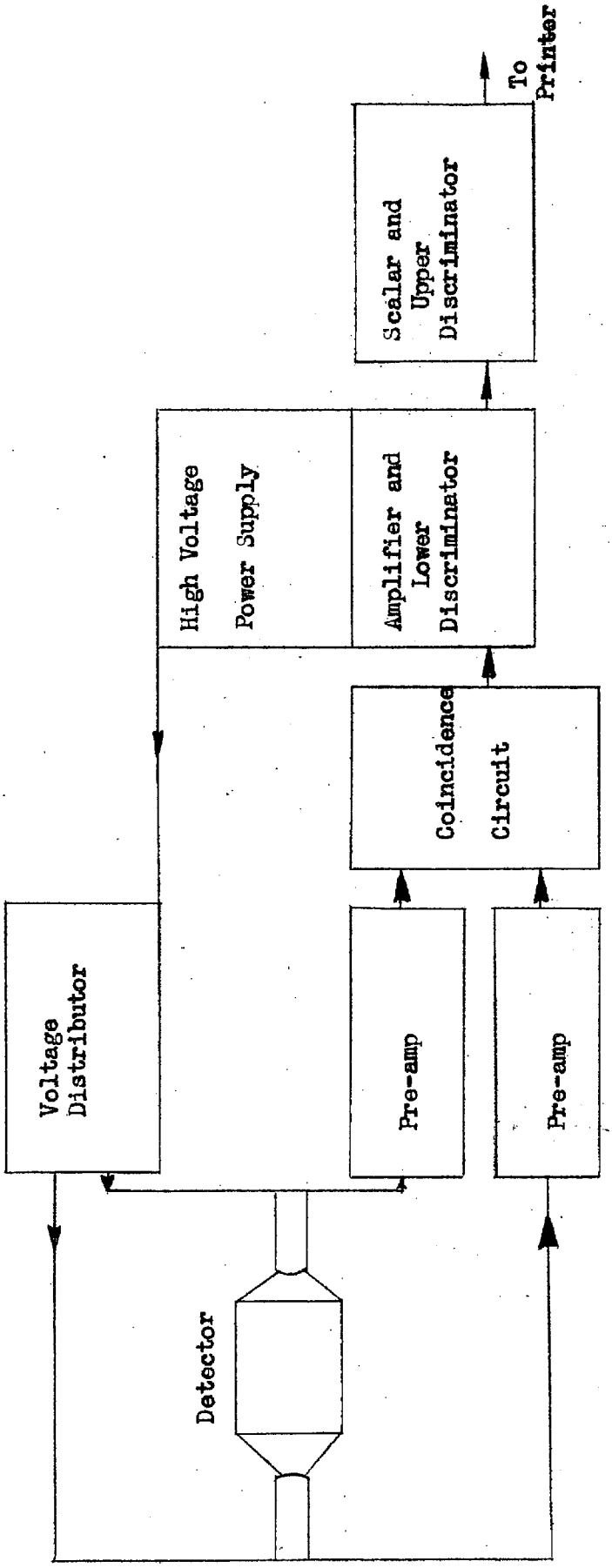

Fig. 20. Functional block diagram of detecting apparatus.

range of energies with mere changes of the controls.

The present problem with regard to the scintillation counter is that of eliminating spurious effects such as changes of pulse height and extra counts. The procedure for determining the presence of extra counts is by the use of the chi-squared test mentioned above. Such a test[21] failed to show any deviation from randomness in the pulses, after certain instabilities and interference effects were eliminated.

Plate 2

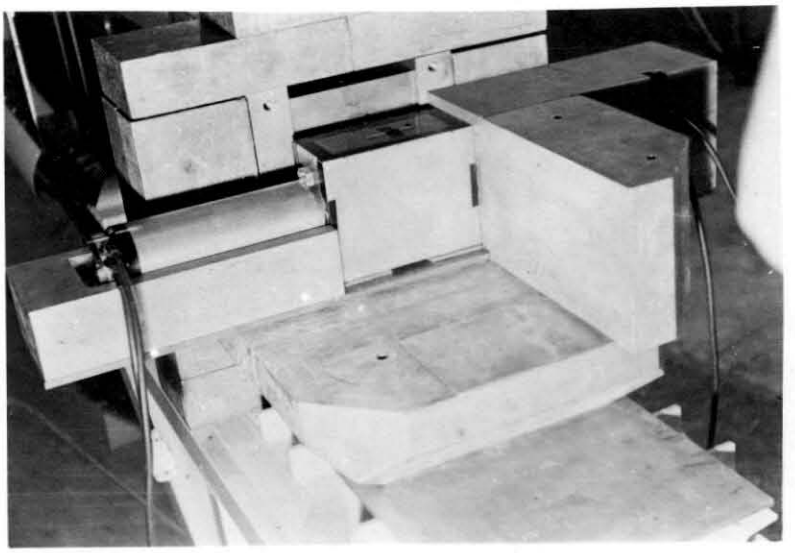

Rear view of scintillation detector assembly for the 2-meter gamma-ray spectrometer with the lead shielding partly removed to show the method of construction.

VI

OPERATION OF THE SPECTROMETER AND ACCUMULATION OF DATA

The design of the curved crystal spectrometer is such that the only practical method of operation is to scan a small region of angular positions, making measurements of the counting rate as function of the angular position. If a gamma ray line is emitted from the source with wavelength corresponding to an angular position within the region under investigation, this line will show up as an increase in counting rate. Thus if counting rate is plotted against angular position or screw position, the lines will show up as curves, typical ones of which are shown in figures 13 and 14.

The procedure for this operation is obvious. The spectrometer is set to a point on its scale, the counting rate is determined by counting for an interval of time, the spectrometer is advanced to a nearby point, the count is again determined, and the cycle is repeated until the region containing the line has been covered. The spectrometer is then moved to the other side of center and the corresponding region on the other side is investigated.

The construction of the spectrometer is such that backlash can exist; hence when a position is set it is always approached from a given direction. This direction corresponds to increasing readings on the screw scale.

The repetitous nature of the procedure has rendered it possible to construct a mechanism for automatic operation, making it unnecessary for the instrument to be attended continuously. It is thus possible to

make maximum use of the life of a radioactive sample. A block diagram of the equipment is given in figure 21. Detailed description is beyond the scope of this paper, but the component parts are the following:

(1) The Timer controls the timing of the sequence of operations. It provides for a given counting interval for each point, to be chosen by the operator. It also provides for printing of the accumulated counts and other information during sub-intervals, in order to provide certain checks on the consistency of counting.

(2) The Screw Set Unit controls the distance through which the wavelength carriage moves between points, hence the location of the points. By the use of a device incorporating a punched tape, a program can be carried out, providing close examination of certain regions of wavelengths, and wider scanning of others.

The screw set unit operates in conjunction with a sector wheel on the screw shaft of the spectrometer, in such a way as to stop the spectrometer accurately at each predetermined position.

A subsidiary function of the screw set unit is a provision for measuring background counting rate at certain intervals by rotating lead blocks into the main beam of gamma radiation.

(3) The Printer accepts and records three pieces of information: time, measured in minutes since a certain reference time; screw setting as indicated by a self-synchronous generator

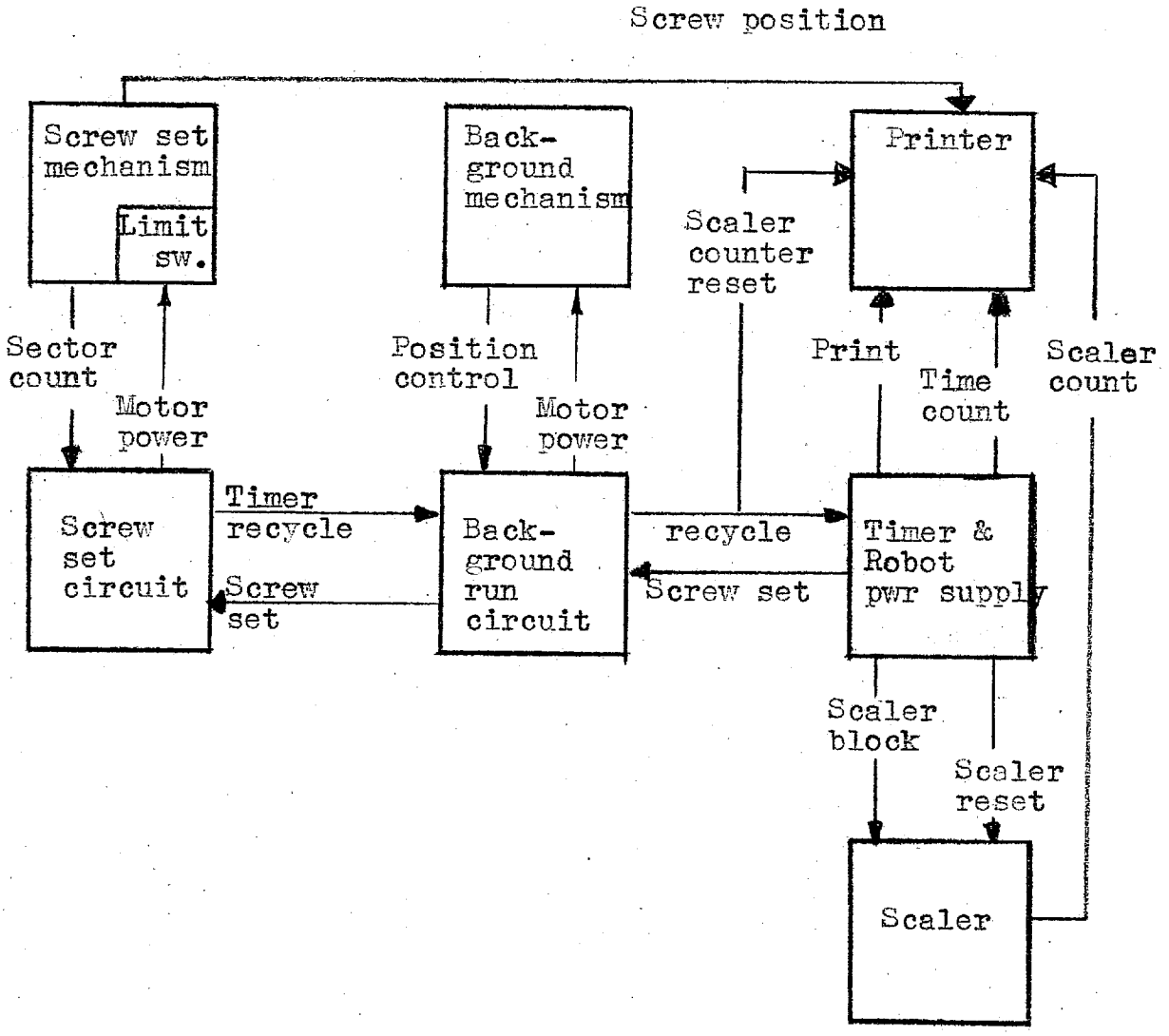

Fig. 21 Robot Functional Block Diagram

on the gear train of the spectrometer screw; and scaler counts. This information is printed at certain sub-intervals, as has been mentioned.

Figure 21 shows the manner in which these units are interconnected and also their connection with units of the scintillation counter.

As a further check on the operation of the instrument, a counting rate meter has been provided, not shown in figure 20, and a Brown recorder prints this counting rate as a function of time. This device has, on occasion, revealed faulty operation of the scintillation counter in the form of erratic counting rate or bursts, and electrical interference from outside sources. It also proves convenient in carrying out preliminary search for gamma-ray lines.

Plate 3

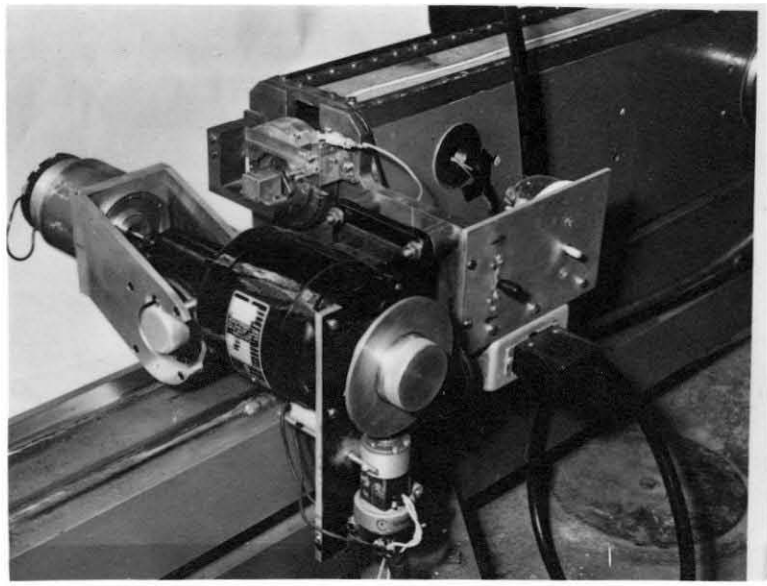

Driving End of Wave-Length Screw Carriage. The large black motor, through a worm gear, drives the wave-length screws (inside the long carriage extending to upper left) when rapid motion over long distances is required. The small vertical motor drives through a friction wheel which is pressed into contact with the friction disc by an electromagnet. This is the robot actuated drive. The selsyn to the left of the large motor transmits the wave-length setting to the robot printer. Above the large motor can be seen the wave-length drum and Veeder-Root counter on which the wave-length setting of the (upper) precision spectrometer screw is read. The toothed contact wheel with alternate insulating and conducting segments and the small gold contact brush riding on its periphery can be seen. These together with the punched programming tape in the robot determine the settings which the robot causes the spectrometer to make.

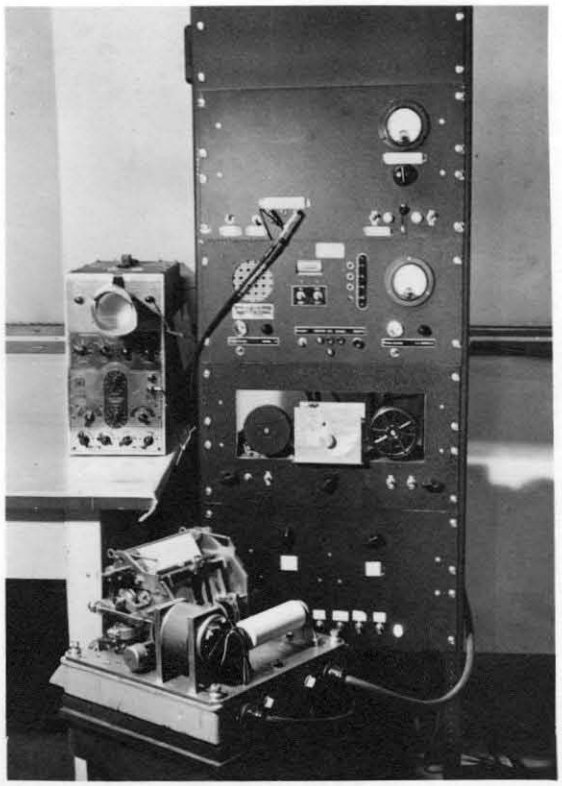

General View of Robot Observer. Designed to cause the 2-meter spectrometer to follow a predetermined program of wave-length settings and to record automatically the gamma ray intensities at these settings over periods as long as 48 hours. The two spools for the programming tape can be seen.

VII

REDUCTION AND EVALUATION OF THE DATA

It has been mentioned above that sufficient data is observed to make possible the plotting of a curve representing the variation of counting rate as a function of wavelength setting of the instrument. Two sets of data are thus recorded, and each of these is subject to certain corrections, some before and others after the curve is plotted.

The counting rate corrections are made before the final plotting of the data. This counting rate contains a background counting due to residual activity in the laboratory, to gamma radiation induced by cosmic ray activity, and to the failure of the shielding to eliminate direct and scattered radiation from the source. For the short region in the immediate neighborhood of a line, this background may be assumed to be a linear function of wavelength position. At long wavelength settings it is, in fact, almost constant, while at short wavelengths, corresponding to 0.2 MeV or higher energy, it has an appreciable slope. The background is determined using points off the spectral line; either graphically, or by a simple average, or in some cases by least squares fitting to a straight line, according to the conditions and precision of the counting measurements. The remaining counting rate is then corrected for decay of the source, in the case of Rn. This is not necessary in the case of RdTh, since the RdTh decays by only 1% in about 10 days.

The counting rate is then normalized in order to make it possible to match curves, and a minor correction of the order of 0.001 milliangstrom is applied to the nominal settings in order to account for the fact that the robot mechanism does not set the screw to the exact setting indicated by the controls, but exhibits a minute periodic error. Curves are then plotted, in preparation for the matching process to be described.

The separations of the lines as reflected on the two sides of the instrument were determined by a matching method originated by D. E. Muller[21]. If a number of observed lines were of the same shape (as in the case of gamma ray lines where the natural spectral line breadth is negligible), a prototype was constructed by normalizing them approximately to the same height, superposing them, and drawing an average curve through their points. A vertical fiducial mark was placed on the prototype and it was then slid over each of the curves in turn, to obtain a best fit. The location of the fiducial mark on the position coordinate of the line-profile was then recorded. In this way the difference between the positions of the line on the two sides of the center of the instrument could be most accurately determined, without the necessity of locating an exact center of each line profile. The fiducial mark was made near the center of symmetry of the prototype in order that the small periodic screw correction (which we apply to the line profile position as a whole rather than to individual settings) should be closely correct.

If only a very few pairs of profiles, such as one or two, were obtained which took the same shape, the pairs were superposed and vertical marks were simultaneously placed on them when the best

fit had been obtained. The difference between a pair of such marks was the required difference of two positions of the same line. It was found that in all cases the line profiles were closely symmetrical, so that asymmetry was not a source of difficulty in the matching process. Asymmetry in the source window or in the crystal curve would not cause difficulty in matching, but any asymmetry due to incorrect slope of the background correction or due to the presence of a fringe of Compton scattered (slightly degraded) radiation would be of a type which could cause mismatch. The latter has been shown to be negligible[22].

The instrument has been designed in such a way that the wavelength of radiation in milliangstroms should be closely equal to readings on the scale, measured in turns of the screw. Small deviations from this rule exist, and the necessary corrections together with the methods by which they have been determined, have been described in previous papers[6]. They are the following:

(1) An aperiodic error which is a smooth function of position,

(2) An error which is roughly a periodic function of the angle of the screw shaft, repeating itself once per turn,

(3) A correction for changes in level of the source table, which could result from imperfections on the carriage tracks or wheels, such as particles of dust,

(4) A constant factor, 1.001,85 expressing the number of milliangstroms per turn of the screw.

These corrections were applied directly to the difference between the readings on the two sides of zero, in the case of each gamma ray line, to yield a corrected value of twice the wavelength.

Use of the relation,

$$E = (12396.44 \pm 0.174) \times 10^{-8} \text{ cm electron-volts}^{22}$$ gives the photon energy of the gamma radiation, if appropriate units are used.

The estimate of the error in wavelength measurement is not a straightforward problem. If we assume that the above-mentioned corrections account for all of the systematic errors, the residual error must result from indeterminacy in matching the curves. The precision with which the curves can be brought into coincidence has been studied by D. E. Muller[10] and a typical result is the following, for a line profile of the shape of an isosceles triangle of height h, placed on a background b, where h and b are measured in counts per minute; and of base width w, where w is expressed in divisions of the screw:

$$p = \frac{4\,h\,t}{w^2} \ln\left(1 + \frac{h}{b}\right)$$

here t is the time in minutes required for counting over the triangular part of the line, and $p^{-1/2}$ is the standard deviation in wavelength setting resulting from a large number of trials at matching this curve to another similar to it assuming that deviations result from the statistical indeterminacy of counting. For the 510 KeV line of ThC", one of the worst cases, with high background and low line height, in which 21 minute runs were made and the line was approximately 10% of background, the measure of precision is given by $p = 3.08 \times 10^5$, and hence the standard deviation is .0018 turns. Since we are combining two runs separated by twice the wavelength, the standard error in

wavelength introduced by the matching is .0013 turns, provided that we regard the counting statistics as good.

Another very important check of the precision of the instrument is its reproducibility. Wherever possible, recurrent runs were made on certain lines of radiation, and reproducibility of their determinations was checked. Failure to reproduce could be caused by a number of effects, but the most likely source of trouble is friction in the main pivot. It is necessary to give some attention to this pivot, oiling it and maintaining correct adjustment. Stickiness in the pivot presumably results in a minute twisting of the shaft which carries the crystal, and manifests itself as a shift in the position of the line on either side. If we picture the source beam as dragging the crystal with it, then as the screw is advanced toward a line the crystal will be pushed in the same direction by the friction, with the result that the line will appear late, i.e. at a higher reading of the screw dial. The opposite effect could occur if the crystal shaft were dragged by the cone bearing attached to the frame of the spectrometer, but only if the lower beam were either elastic, or not tightly attached to the vertical shaft, so that the twisting motion could be transmitted from the lower part of the shaft to the crystal at the top.

Examination of the reduced data, in particular of the 52.8 KeV line of Rn, showed that such an effect was taking place, but the deviations were so evenly distributed as to make it impossible to decide which of the abovementioned possible effects might be predominant. The deviations are approximately 0.02 milliangstroms, and are quite

serious at high energy. Oiling the upper cone of the main pivot seemed to reduce this effect, but appropriate allowance will be made for it in assigning probable errors. Since this error is much larger than error due to matching of the curves, and is larger than the screw corrections, it will contribute by far the greatest portion of the assigned probable error.

VIII

RESULTS OF MEASUREMENT OF THE GAMMA RADIATION FROM THE RADIUM DISINTEGRATION SERIES

8.1 The Observed Wavelengths and their Probable Errors

Five samples of Rn gas (half life 3.8 days) have been used in the determination of the gamma ray wavelengths of the radium series. In each case it was possible to make measurements continuously for one to two weeks, depending on the strength of the sample. The line strengths were sufficient to insure good counting statistics; the 241 KeV line, the weakest to be measured, rose to about 30% above the background counting rate while the 53 KeV line provided the best contrast, with its peak 3.5 times as high as background (with a source of 100 millicuries).

The data have been reduced in the manner described in Part VII, and the results of the individual runs have been presented in Table I. The wavelength in milliangstroms has in each case been obtained by applying the screw corrections to the observed positions of the lines. Many runs were made whose results do not appear in this table. In some cases they were only partly successful because of erratic behavior of the equipment, while in other cases they simply were inferior in quality because they were shorter or because they were measured through the use of the Geiger counter and their quality was overshadowed by newer runs using the scintillation counter.

The method of assigning probable errors has proven to depend entirely on the internal consistency of the results of the individual determinations since we believe we have removed all comparable systematic

errors. If n measurements x_i are made, all of equal weight, and if δx_i are the deviations of the individual values from their mean, then the standard error* of a single observation is[24]

$$\delta x_i = \sqrt{\frac{\Sigma(\delta x_i)^2}{n-1}} \qquad \text{eq. (1)}$$

while the standard error of the determination (whose value is taken to be the mean of x_i) is

$$\delta x_m = \sqrt{\frac{\Sigma(\delta x_i)^2}{n(n-1)}} \qquad \text{eq. (2)}$$

This value has been obtained in each case for which several runs were made on a given line. Since the anticipated deviation due to matching the curves with the statistics available at present is very small (about 1/10) compared with the standard deviation of one observation, we feel justified in neglecting the deviation due to the matching of curves, in the assignment of standard error. This has the effect of giving all of the runs on a given line equal weight as long as they have counting statistics which afford a precision of matching corresponding to 0.003 milliangstroms or better. This is true in the case of all runs listed in Table I, since a sufficient number of runs were made on each line to permit discarding of the inferior runs.

Thus a standard deviation for a single observation has been calculated for runs on each of the lines. It is assumed that the reproducibility in wavelength of the spectrometer is the same for

---

* For a normal distribution of errors, the standard error is related to the probable error through the factor 0.6745. Since we may not have a normal distribution, we shall adhere to the use of standard errors and deviations, and the factor 0.6745 will not appear in our expressions.

Table 1

Wavelengths of Observed Gamma Rays of RaB-RaC and RaC-RaC':

Results of Individual Measurements (wavelengths in milliangstroms)

Nominal Energy of the Line, and Run Number		Observed Wavelength of Run	Mean-Observed Wavelength on this Line	Standard Error of a Single Measurement
53 KeV	#2	232.880	232.881	.0092
	#3	232.891		
	#4	232.872		
241 KeV	#1	51.252	51.246	.008
	#2	51.258		
	#3	51.228		
294 KeV	#2	42.018	41.999	.0134
	#4	41.995		
	#5	41.992		
	#6	41.989		
350 KeV	#4	35.241	35.231	.0078
	#3A	35.228		
	#4'	35.226		
607 KeV	#1	20.366	20.365	.0174
	#2A	20.379		
	#3A	20.343		
	#5	20.346		

Table 2

Energies and Intensities of Gamma Rays of the Radium Series

Ellis et al., Energy, KeV	Present Observed Energy, KeV, Together with Standard Error	Present Observed Relative Intensity
	RaB-RaC Transition	
52.9	52.231 ± 0.002	
240.6	241.90 ± 0.04	.2
293.7	295.16 ± 0.05	.55
349.9	351.857 ± 0.081	1
	RaC-RaC' Transition	
606.7	608.7 ± 0.2	1.6

all wavelengths, so that the standard error of a single observation should be the same for any wavelength. Therefore the standard error of an observation has been taken to be the weighted root-mean-square value of the abovementioned individual standard errors of a measurement on each individual line. In this manner we have found the standard error of a measurement of a line of the Rn source to be .013 milliangstroms. The standard error of a determination consisting of the mean of n measurements of a line has been taken to be $1/\sqrt{n}$ times this value.

The final values of the quantum energies of these five lines are presented in Table 2, together with the standard errors in energy as determined from the abovementioned assigned errors.

8.2 Estimated Relative Intensities of the Lines

Approximate comparison of the intensities of two lines can be made by correcting the relative line heights for (1) decay of the source between measurements, (2) the relative reflection coefficients of the crystal for the two energies, and (3) the relative sensitivity of the detector for the two energies. It was not necessary to take into account the absorption of the Al tube, for it is only 3% for the 53 KeV radiation, the worst case.

We have selected for comparison of line intensities the measurements on the first source, using the Cu-cathode Geiger counter. The reflection coefficient of the crystal has been shown[25] to be proportional to λ^2, where λ is the wavelength. A curve has been calculated showing the behavior of the efficiency of the Cu counter in the range of interest, and it is presented in figure 22. We do not attempt to compare the intensity of the 53 KeV line with the other lines because of the difficulty of estimating the relative efficiency of the

scintillation counter over such a wide range of quantum energy. The relative intensities are presented in Table 2.

8.3 The Search for Weaker Lines

Intensity calculations predicted that the 766 KeV line of RaC-RaC' would be about 5% as strong in counting rate as the 607 KeV line. A search was carried out using one of the standard programming tapes on the site of the 766 KeV line. In spite of erratic behavior of the scintillation counter, a small indication of a line was observed. It was concluded that no improvement could be gained over the previously published value of the energy by measuring such a weak line, and the search was not carried further.

The other lines of RaC-RaC' are estimated to be much weaker than even the 766 KeV line, so that the hope of detecting them in the near future is very small.

8.4 The x-ray Lines of Bi and Po

Examination of the decay scheme of the uranium series discloses that the x-rays of $_{83}RaC^{214}$ and $_{84}RaC'^{214}$ should be present as a result of internal conversion of the gamma rays. We have found and been able to identify in published tables[26] the following x-ray lines of $_{83}Bi$: $K\alpha_2$, $K\alpha_1$, $K\beta_3$, $K\beta_1$, $K\beta_2^{II}$, and $K\beta_2^{I}$. In addition we have detected another line, which we believe to be the $K\alpha_1$ line of $_{84}Po$. Since the published values of the Bi x-ray lines show precision well within the precision of the curved crystal spectrometer, we feel that the best value of the wavelength (in XU Siegbahn) is obtained by using the instrument to measure the difference in the wavelengths of the Po and Bi lines, comparing the Po $K\alpha_1$ line

with the Bi $K\alpha_1$ line. This has been done, and after screw corrections are applied, there results the following value of the wavelength of the Po $K\alpha_1$ line:

$$\lambda = 156.601 \pm .010 \quad \text{XU (Siegbahn)}$$

8.5 The Decay Scheme of the RaB-RaC Transition

Stern[27] and others have given a decay scheme showing the energy levels of RaC in the RaB-RaC β-decay transition (fig. 28). It will be seen that all of the gamma rays shown in the scheme have been measured in the present work. The .056 MeV transition is evidently a non-radiative (completely internally converted) transition, for no such gamma ray has been previously reported, and we were unable to find any in a search conducted by the use of the counting-rate meter.

If our measurements are to be compatible with this decay scheme, the new determinations of the 241 KeV line, the 53 KeV line, and the 294 KeV line must show closure. Using the energies of the lines given in Table 2, we find that

$$(241.90 \pm .04) + (53.231 \pm .002) +$$
$$- (295.162 \pm .05) = .031 \pm .064$$

so that the decay scheme is verified within our experimental error.

Since we have measured only one line of the RaC-RaC' transition, this work has no bearing on the validity of any decay scheme for that transition.

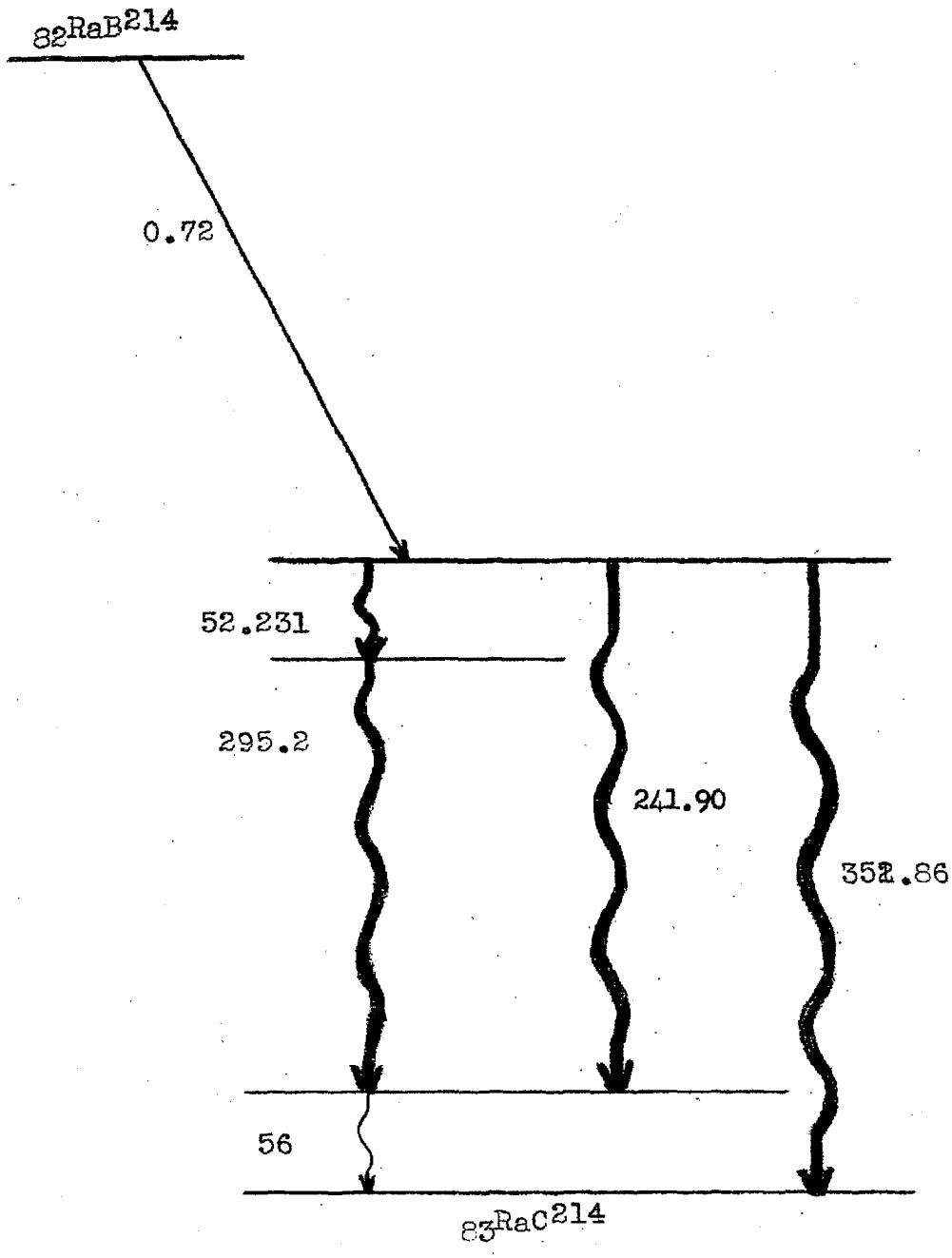

Fig. 23. Energy level diagram of RaB-RaC. The heavy lines indicate transitions studied in the present work. The 56 KeV transition is presumed to be a non-radiative transition.

IX

RESULTS OF MEASUREMENT OF THE GAMMA RADIATION OF THE THORIUM DISINTEGRATION SERIES

9.1 The Observed Wavelengths and their Probable Errors

A single source of RdTh (half life 1.9 years) described in Part III was used in the measurements of the thorium series radiation. These measurements were carried out over a period of six months, with work on other radioisotopes interspersed with them. As was mentioned in Part III, this source was not well suited to the geometry of the instrument, nevertheless it was possible to make measurements of some of the lines of this rich spectrum despite low intensity and the presence of high background.

The data have been reduced and standard errors assigned by the methods described in Part VII and Part VIII. In all cases except that of the 726 KeV line, the error of matching profiles is thought to be smaller than the total probable error, so that with repeated measurements on certain of the lines, the error is assigned on the basis of internal consistency. For such runs the standard error of a single measurement is 0.011 milliangstroms, in substantial agreement with the standard error of a measurement listed above for the case of Rn. In the case of the 726 KeV line, it was only possible to make two runs, both on the positive reading side of the instrument, as the scintillation counter was behaving badly. Consequently we have the possibility of a systematic error due to indeterminacy of the zero position of the scale. In addition the line was weak, being superposed on the high background due to the hard radiation of ThC'',

and it was therefore considered advisable to double the experimental error to be assigned to this wavelength.

The results of the individual measurements are presented in Table 3, as well as the standard error of the determination of each line. The final values of the quantum energies appear in Table 4.

9.2 Relative Line Intensities

In order to compare the intensities of two lines it is necessary to correct for (a) self absorption in the source and absorption in the platinum-iridium capsule, (b) change in line-height resulting from difference of size of the slit, if any for the two lines, (c) the different reflection coefficients of the crystal for the two energies, and (d) the different sensitivities of the scintillation counter for the two energies.

A curve has been prepared (fig. 24) giving the attenuation factor due to self-absorption of the source and absorption in the container. Since almost all of the runs were made with the use of a 0.005" slit gap, it is possible to obtain ratios without the correction for the slit gap. If necessary, the relative line height could be taken from the generating function curve, figure 12. For our purposes we assume that the efficiency of the scintillation counter is proportional to the absorption of the radiation by the NaI scintillating crystal. A curve has been prepared (fig. 25) which gives the absorption in this crystal as a function of energy.

The relative intensities of the observed lines are given in Table 4, together with their energies.

Table 3

Results of Individual Observations of the Gamma Rays of the Thorium Series. (Wavelengths in Milliangstroms)

Nominal Energy of Line	Observed Wave-Length of the Run	Mean of All Runs on this Line	Standard Error of a Single Measurement
238 KeV	51.979	51.971	0.011
	51.963		
241 KeV	51.461	51.455	0.0092
	51.448		
276 KeV	44.703	44.703	
510 KeV	24.330	24.292	0.012
	24.283		
580 KeV	21.279	21.279	
726 KeV	16.98	16.99	0.02
	17.00		

Table 4

Energies and Intensities of Gamma Rays of the Thorium Series

Ellis et al., Energy, KeV	Present Observed Energy, KeV and Standard Error	Present Observed Relative Intensity
	ThB-ThC Transition	
237.9	238.52 ± 0.036	1
	ThC-ThC' Transition	
726	729.6 ± 0.9	.15
	ThC"-ThD Transition	
276.5	277.308 ± 0.07	.05
510.0	510.30 ± 0.16	.15
582.3	582.57 ± 0.3	.4
	Unassigned	
	240.92 ± 0.036	.1

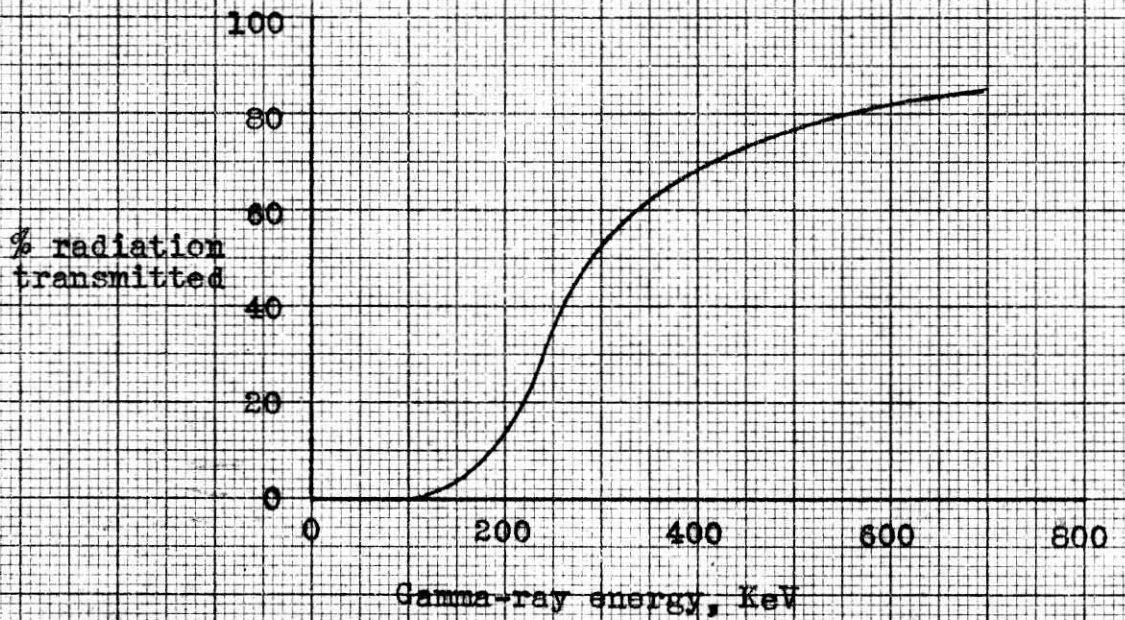

Fig. 24 Attenuation factor due to self absorption and absorption in the platinum-iridium container, for the RdTh source (calc.)

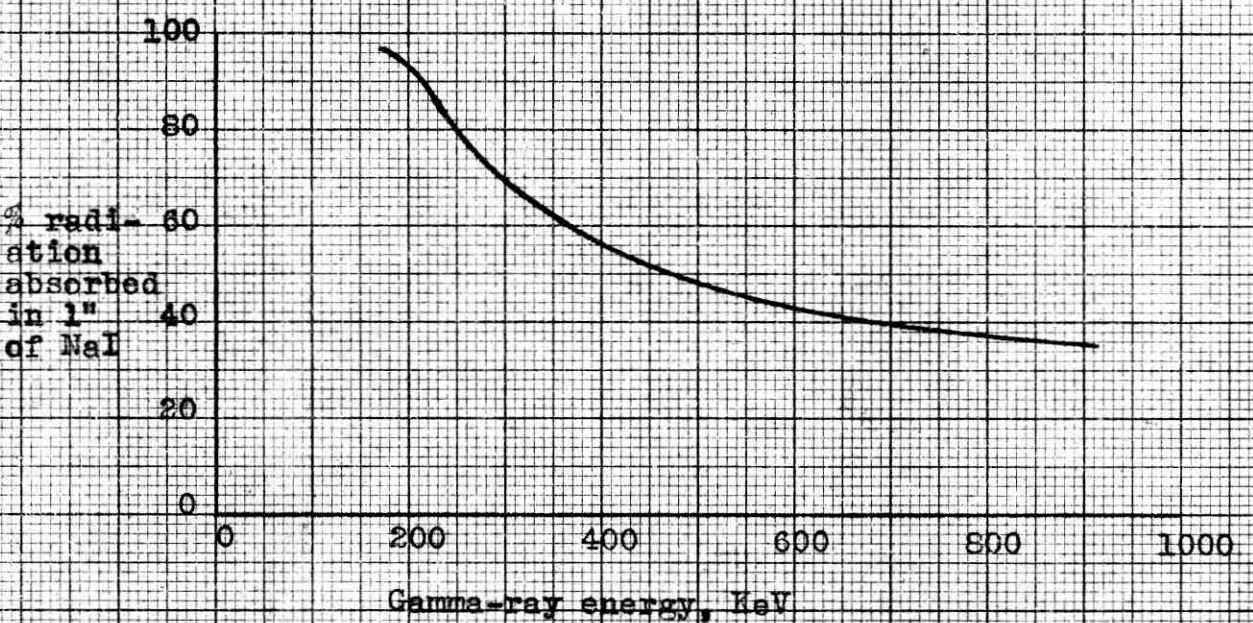

Fig. 25 Absorption of gamma rays in the scintillating crystal, NaI 1" thick

9.3 The Search for Weaker Lines

After the six lines reported here had been measured, attempts were made to find certain other lines which were considered promising on the basis of intensity calculations. A search was made for the 617 KeV line of ThC, counting for 21 minutes on each point, but the counting statistics did not permit a definite indication of the line.

Several attempts were made to find the hard (2.62 MeV) line of ThC". The line is very strong, being emitted in 34% of the disintegrations. However the reflection coefficient of the crystal is so small at this short wavelength, and the background radiation is so high due to proximity of the main beam of radiation, that it was impossible to obtain a definite indication of the line. Figure 26, showing the curve of background as a function of screw reading near the center of the instrument, illustrates the difficulties encountered in measurement of such a high-energy line. Its position is barely outside of the design "window" of the collimator.

In addition a search was made, using the counting rate meter, of the entire region from 10 to 100 milliangstroms. This method of search, used so effectively in the study of other radioisotopes, failed to show even previously measured lines. It showed only the 238 KeV line and passed over the others listed in Table 3.

9.4 The Decay Scheme of the ThC"-ThD Transition

The most recent energy level diagram of ThD is given[28] in figure 27. The lines which have been measured in the present work are indicated. There are no closure relations between the lines which we have measured.

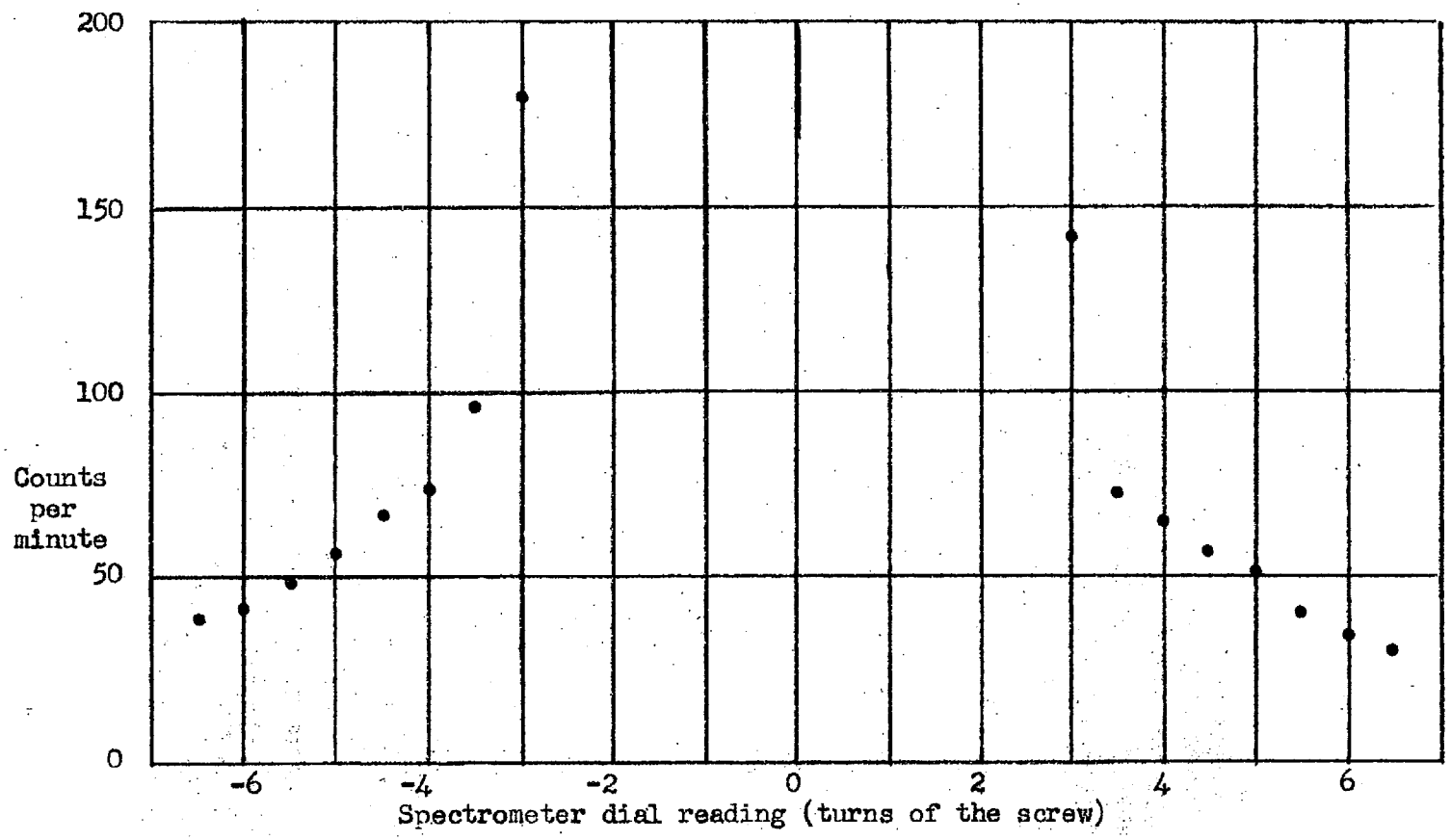

Fig. 26. Counting rate near the center of the spectrometer, showing the high background in the vicinity of the assumed position of the ThC" 2.62 MeV line (arrow). In the center portion of this plot, the counting rate would be extremely high since the detector accepts the main undiffracted beam of radiation.

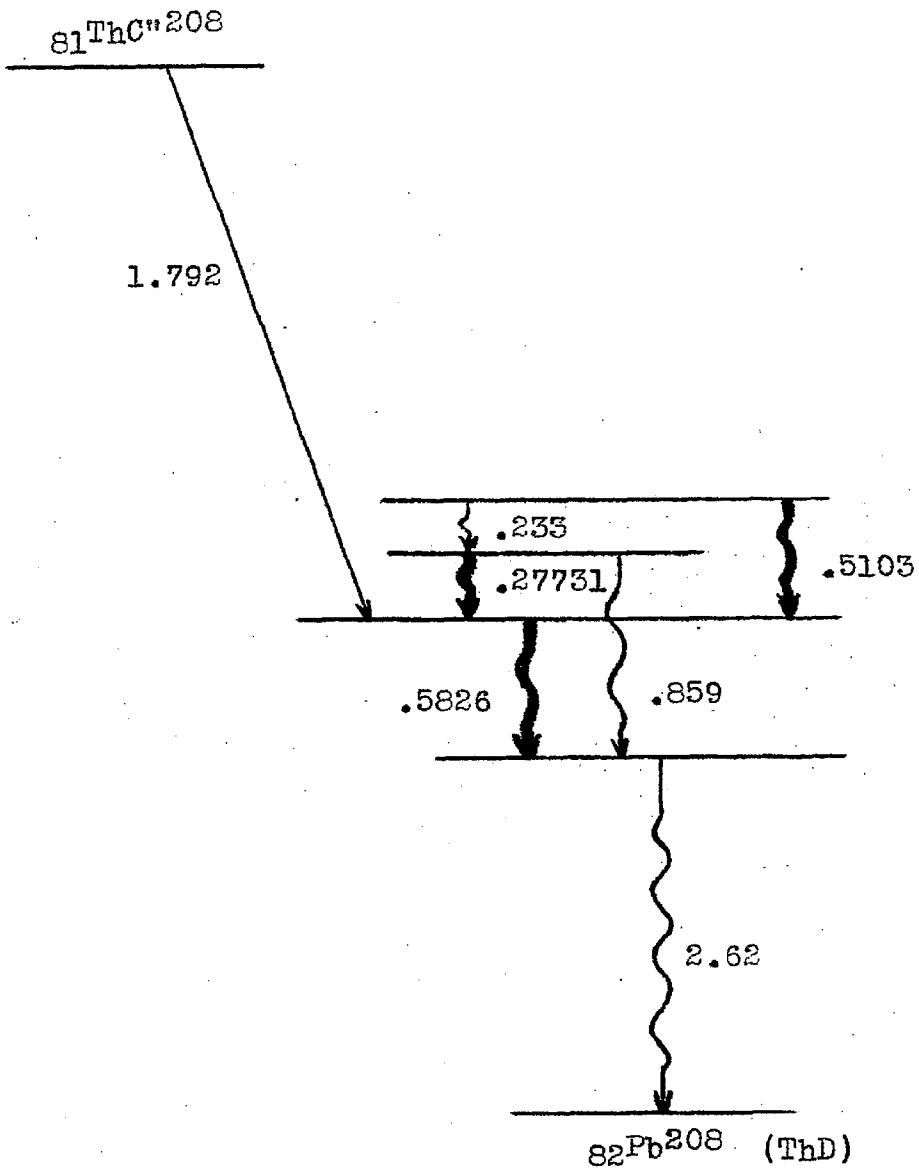

Fig. 27. Decay of ThC"-ThD (H. O. W. Richardson). Heavy waved lines indicate gamma-ray transitions reported in the present work.

The other two lines which were measured occur with different transitions; the 238 KeV line accompanies the ThB-ThC transition while the 726 KeV line accompanies the ThC-ThC' transition.

9.5 The 241 KeV Line

A study of the literature has failed to show previous reports of a gamma ray of 241 KeV in the thorium series. This line is very close to the 241 KeV line of RaB, consequently the idea was advanced that the Th sample may contain Ra as an impurity. However a search for other lines of RaB in the Th sample has failed to show the 294 KeV or 350 KeV line of RaB. Furthermore the observed difference between the wavelengths of the two 241 KeV lines is 0.25 milliangstroms, more than ten times the probable error of a determination. Since this line is approximately 10% as strong as the 238 KeV line and only 1% different in energy, it may not be unreasonable to assume that it was not resolved by the beta-ray spectrometers which have made the previous measurements of the radiation of the thorium series. We have as yet been unable to find a place for this line in the decay scheme of the thorium series.

REFERENCES

(1) Rutherford and Andrade, Phil. Mag. 27 854; 28 263 (1914)

(2) M. Frilley, Annales de Physique 11 483 (1929)

(3) M. J. N. Valadares, Annales de Physique Ser 11 2 197 (1954)

(4) DuMond, Rev. Sci. Inst. 18 626 (1947)

(5) DuMond, Lind and Watson, Phys. Rev. 75 1226 (1949)

(6) J. R. Brown, Thesis, Calif. Inst. of Tech. (1951)

(7) Rasetti, Elements of Nuclear Physics, New York, Prentice-Hall, (1936), p. 125 et seq.

(8) W. G. Cross, Thesis, Harvard Univ., 2 Dec. 1949, describes the source, and research done using it.

(9) Cross and Ramsey, Phys. Rev. 80 929 (1950) describes the same work as (8) in shortened form.

(10) H. B. Dwight, Tables of Integrals, New York, Macmillan, 1947

(11) Lind, Rev. Sci. Inst. 20 255 (1949)

(12) Lind, Brown and DuMond, Phys. Rev. 76 1838 (1949)

(13) Paetow, Zeits. f. Phys. 111 770 (1939)

(14) Norling, Arkiv. f. Math. Astr. och Fys. 27A no. 27 (1941)

(15) W. Heitler, Quantum Theory of Radiation, Oxford Univ. Press, 2nd edition (1944)

(16) Bradt, Gugelot, Huber, Medicus, Preiswerk, and Sherrer, Helv. Phys. Acta 19 77 (1946)

(17) Curves used as course material by Prof. William A. Fowler, Calif. Inst. of Tech. 1947

(18) Hoel, Introduction to Mathematical Statistics, New York, Wiley (1947). See Chap. X and Table III.

(19) J. R. Brown, Thesis, loc. cit. fig. 24

(20) Gaelen L. Felt, Thesis, Calif. Inst. of Tech., (1951)

(21) D. E. Muller, Thesis, Calif. Inst. of Tech., (1951)

(22) DuMond, Phys. Rev. 75 1266 (1949)

(23) DuMond and Cohen, A Least-Squares Adjustment of the Atomic Constants as of December 1950, Calif. Inst., Report to the NRC Committee on Constants

(24) Handbook of Chemistry and Physics, Cleveland, Chemical Rubber Publishing Company, see the explanation of the Mathematical Tables.

(25) Lind, West and DuMond, Phys. Rev. 77 475 (1950)

(26) Cauchois and Hulubei, Longueurs d'Onde des Emissions X, etc., Paris, Hermann & Cie, (1947)

(27) M. Stern, Rev. Mod. Phys. 21 316 (1949)

(28) Nuclear Data, Bureau of Standards Circular 499